Implementing plant hydraulics in the Community Land Model

Daniel Kennedy[1], Sean Swenson[2], Keith W. Oleson[2], David M. Lawrence[2], Rosie Fisher[2], Pierre Gentine[1]

[1]Columbia University, New York, NY 10027 USA
[2]National Center for Atmospheric Research, Table Mesa Drive, Boulder, Colorado, USA

Key Points:

- An updated soil-plant-atmosphere continuum model based on hydraulic theory is implemented in the Community Land Model (version 5).
- Prognostic leaf water potential replaces soil matric potential as the basis for stomatal conductance water stress.
- Prognostic root water potential is used to implement hydraulic root water uptake, replacing the heuristic soil 'wilting' point.

Corresponding author: Daniel Kennedy, `djk2120@columbia.edu`

Abstract

CLM5 introduces the Plant Hydraulic Stress (PHS) configuration of vegetation water use, which is described and compared with the corresponding parameterization from CLM4.5. PHS updates vegetation water stress and root water uptake to better reflect plant hydraulic theory. The new configuration introduce prognostic vegetation water potential to the CLM, modeled at the root, stem, and leaf levels. Leaf water potential replaces soil matric potential as the basis for stomatal conductance water stress, and root water potential is used to implement hydraulic root water uptake, replacing a transpiration-partitioning heuristic. Point simulations of a tropical forest site (Caxiuanã, Brazil) under ambient conditions and partial precipitation throughfall exclusion are carried out to highlight the differences between PHS and the previous plant hydrodynamics scheme.

1 Introduction

Trees face emerging climate change risk globally [*Allen et al.*, 2010; *Anderegg et al.*, 2013a]. In addition to stress from soil moisture drought, vegetation is susceptible to increasing atmospheric demand [*Restaino et al.*, 2016; *Novick et al.*, 2016a; *Lemordant et al.*, 2018]. Increases in vapor pressure deficit (VPD) are occurring with global warming [*Ficklin and Novick*, 2017; *Seager et al.*, 2015], and are associated with impacts on vegetation such as large-scale die-off [*Williams et al.*, 2013; *McDowell and Allen*, 2015]. Understanding vegetation response is important both for discerning future climate impacts on forests and for modeling feedbacks to the carbon and hydrological cycles [*Lemordant et al.*, 2018]. Significant uncertainty remains in Earth System model predictions of the carbon cycle caused by the response of vegetation to changes in hydroclimate [*De Kauwe et al.*, 2017; *Friedlingstein et al.*, 2014; *Trugman et al.*, 2018].

Plant water stress parameterizations are used by Earth System Models to determine the regulation of surface fluxes (photosynthesis, transpiration) by vegetation in response to water fluctuations [*Egea et al.*, 2011; *Verhoef and Egea*, 2014]. These parameterizations, which relate a metric of soil moisture status to leaf gas exchange, are widely used to define the response of stomatal conductance to vegetation water status, serving to attenuate transpiration, photosynthesis, and root water uptake with drying. Because vegetation water use strategies modulate carbon uptake, creating a close coupling between the Earth System's carbon and hydrological cycles [*Green et al.*, 2017], the dynamics of the water stress representation in models have broad effects on critical land surface processes [*Joetzjer et al.*, 2014], such as photosynthesis rates. On daily and weekly time scales, water stress parameterizations influence the partitioning of latent versus sensible heat, modifying the Bowen ratio [*Gentine et al.*, 2007, 2011]. This in turn feeds back onto surface and air temperature, through land-atmosphere feedbacks [*Bonan*, 2008; *Seneviratne et al.*, 2006]. On longer timescales vegetation water use strategies regulate the global carbon and water cycles [*De Kauwe et al.*, 2015].

Several recent studies have aimed at advancing the representation of water flow through the Soil-Plant-Atmosphere continuum (SPAC) in land-surface and ecosystem models [*Xu et al.*, 2016; *Christoffersen et al.*, 2016; *Sperry et al.*, 2017] by incorporating plant hydraulic theory. Explicit modeling of water flow through the vegetation increases model complexity, but is consistent with evidence of dynamic regulation of vegetation water use in response to both soil and atmospheric drying [*Tardieu and Simonneau*, 1998; *Sperry et al.*, 1998; *Sperry and Love*, 2015]. Furthermore, because they are based on Darcy's Law, plant hydraulic models have a robust physical basis compared to models that utilize empirical water stress formulations. Plant hydraulic models involve new parameters, which presents challenges [*Drake et al.*, 2017], but plant hydraulic trait data are available [*Kattge et al.*, 2011; *Anderegg*, 2015a], providing constraints on parameter estimation. Such data have been shown to be informative of species vulnerability to drought [*Choat et al.*, 2012]. Likewise vegetation water status observations are now available from remote sensing platforms, at a scale that is directly comparable to model development [*Konings et al.*, 2016; *Grant et al.*, 2016]

and therefore can be used to validate model results [*Momen et al.*, 2017; *Konings et al.*, 2017b].

In this study, we develop a new plant water stress parameterization based on hydraulic theory within the recently released Community Land Model, version 5 (CLM5, the land component of the Community Earth System Model version 2). We refer to this hydraulics-based implementation as the 'Plant Hydraulic Stress' (PHS) configuration. Previous versions of the CLM, similar to many Land Surface Models, employed an empirical β-form soil moisture stress function. Such functions lack a strong physical basis and have been shown to systematically overestimate the effect of soil moisture drought on evaporative fluxes [*Ukkola et al.*, 2016; *Bonan et al.*, 2014]. In Amazonia, which is the focus area of our model test runs, studies suggest that the CLM (version 3.5) simultaneously underestimates the effect of experimental drought treatment [*Powell et al.*, 2013] and overestimates dry-season reductions in GPP [*Restrepo-Coupe et al.*, 2017].

PHS, by explicitly representing plant hydraulics, introduces modeled vegetation water potential (discretized into leaf, stem and root elements) into the CLM, as well as a physical model of water supply, from the soil through the vegetation substrate. Transpiration is attenuated in the model according to leaf water status, capturing dynamic vegetation water use regulation in response to both soil moisture and atmospheric evaporative demand. These changes in the parameterization framework have numerous implications, including:

1. Leaf water potential serves as a metric for plant water status instead of soil water or soil matric potential. As such, it reflects vegetation sensitivity to both soil and atmospheric drying, while serving as a diagnostic for excessive xylem tension and cavitation risk.
2. Modeling plant hydrodynamics allows representation of hydraulic redistribution [*Lee et al.*, 2005], as the flow respects Darcy's law and thus is always directed down gradients of water potentials.
3. Root water potential can be used to predict gradient-based root water uptake based on Darcy's law, replacing the previous empirical transpiration partitioning heuristic. This provides the means to vary, for example, the mean depth of extraction with changing soil water conditions.
4. Representation of a range of water use strategies (i.e. isohydricity and anisohydricity), improving the connection between plant carbon allocation and water availability.
5. Modeling vegetation water potential allows improved connection to remote sensing observations of vegetation water status (Vegetation Optical Depth) [*Konings et al.*, 2016].

To assess the new model formulation, we carried out site-level simulations at Caxiuanã National Forest in Brazil, which features a critical biome (terra-firme moist tropical evergreen forest) [*Fisher et al.*, 2006]. Starting in 2001, a plot at this site was subjected to an approximately 50% percent precipitation throughfall exclusion. Due to the large drop in soil moisture at the precipitation exclusion site, significant vegetation water stress regulation of transpiration and photosynthesis was observed at the site, providing an interesting test for the model [*Fisher et al.*, 2007].

In this paper we therefore:

1. Introduce the PHS theory and implementation in the CLM (Section 2)
2. Describe the details of the experiment setup (Section 3)
3. Analyze the dynamics of modeled water stress, root water uptake, transpiration, and soil moisture profiles (Section 4)
4. Discuss differences between PHS and the previous CLM water stress configuration (Section 5)
5. Outline the benefits and limitations of the new model (Section 5.7)

2 Model Description

This study uses CLM5 to compare two parameterizations of water stress (Sections 2.4.1 and 2.5.1) and root water uptake (Sections 2.4.2 and 2.5.2). The first parameterization, which we refer to as Soil Moisture Stress (SMS), deploys the CLM4.5 default root water uptake and water stress implementations within CLM5. The second is called Plant Hydraulic Stress (PHS); PHS is the default configuration of CLM5. In Sections 2.1-2.3, we describe the components that the two configurations share in common. In Sections 2.4 and 2.5, we describe their differences.

2.1 Stomatal Conductance

CLM5 implements the Medlyn stomatal conductance model, which reconciles the empirical and optimal approaches to stomatal conductance [*Medlyn et al.*, 2011]. Such "optimal" stomatal conductance models serve to maximize photosynthesis relative to transpiration costs. Stomatal conductance of CO_2 (g_s) is directly related to net photosynthesis (A_n) and inversely related to the square root of the vapor pressure deficit near the leaf surface ($\sqrt{D}$) and the concentration of CO_2 at the leaf surface (C_a).

$$g_s = g_0 + \left(1 + \frac{g_1}{\sqrt{D}}\right)\frac{A}{C_a} \tag{1}$$

The model features two parameters: g_0 (μmol / m^2 / s) and g_1 (kPa$^{0.5}$). The g_0 parameter is the minimum stomatal conductance, representing cuticular and epidermal losses (small). The g_1 parameter relates to the marginal water cost guiding the optimization of carbon assimilation. These parameters are plant functional type dependent.

While maximizing assimilation relative to water transpiration costs ($A - \lambda E$), the Medlyn model does not resolve concurrent limitations to stomatal conductance associated with declining soil water. To represent soil water stress, and its impact on leaf-gas exchange, land surface models typically include a 'water stress factor'.

2.2 Photosynthesis

The CLM5 photosynthesis model is described in detail in *Bonan et al.* [2011], *Thornton and Zimmermann* [2007], and *Oleson et al.* [2013]. Photosynthesis is limited by three factors: carboxylation-limitations, light-limitations, and export-limitations following *Farquhar et al.* [1980] and *Harley et al.* [1992]. Water stress (as discussed in the next section) is applied within the carboxylation-limited regime, by attenuating the maximum rate of carboxylation (V_{cmax}). The implementation extends *Sellers et al.* [1996a,b] with co-limitation following *Collatz et al.* [1991].

The CLM5 photosynthesis module, in its default configuration, is a two-big-leaf model, with a sunlit and shaded leaf for each plant functional type [*Thornton and Zimmermann*, 2007; *Dai et al.*, 2004; *Oleson et al.*, 2013]. The canopy fluxes module iterates the solution for leaf temperatures to satisfy the leaf surface energy balances on both sunlit and shaded leaves, in response to forcing conditions. Within this, the photosynthesis module further iterates to solve for stomatal conductance and intercellular CO_2 concentration, balancing stomatal flux of CO_2 with photosynthetic assimilation flux of CO_2 (see Supp Fig B.1 for a flow chart of these iterations).

2.3 Water stress factor

Uncertainty remains within the literature as to how and where to apply water stress factors to photosynthesis and/or stomatal conductance [*Zhou et al.*, 2013; *Novick et al.*, 2016b; *Sperry and Love*, 2015]. In the CLM, the water stress factor (f_w) multiplies the 'well-watered rate' of maximum carboxylation ($V_{\text{cmax,ww}}$) to effect water stress (as described in *Oleson et al.* [2013]).

$$V_{\text{cmax}} = f_w \, V_{\text{cmax,ww}} \qquad (2)$$

Attenuating V_{cmax} is not the only method for incorporating a response to declining water availability. Other models opt to apply water stress directly to stomatal conductance, linking the stomatal conductance model slope parameter to soil moisture (e.g. *De Kauwe et al.* [2015]). However, *Lin et al.* [2018] found that only the intercept parameter and photosynthesis (through changes in light-use efficiency) were sensitive to soil moisture based on eddy-covariance observations and not the slope parameter. Furthermore *Zhou et al.* [2013] suggest that changes in assimilation tend to exceed those predicted by modulating g_1 with soil moisture, but could be captured by changing V_{cmax}. These results would thus suggest that it is appropriate to modulate V_{cmax}. Other field studies, however, suggest that measured V_{cmax} at the leaf level does not change with drought [*Flexas et al.*, 2004]. On the other hand, the modeled V_{cmax} is a bulk measure of V_{cmax} and may implicitly account for mesophyll conductance changes [*Rogers et al.*, 2017], which has been shown to be water stress dependent [*Flexas et al.*, 2012].

For now, applying water stress through V_{cmax} seems well-supported, but future refinements may be appropriate. In this study, we preserve the method of applying water stress used in CLM4.5, while instead experimenting with how f_w responds to environmental conditions.

2.4 SMS (CLM4.5 default)

2.4.1 SMS Water Stress Factor

In SMS, the water stress f_w is calculated as the summation of a soil layer wilting factor (w_i) across the n soil layers, weighted by root fraction (r_i) [*Oleson et al.*, 2013]. The soil wilting factor is a bounded linear function of soil matric potential ($\psi_{\text{soil},i}$). The function is defined by two parameters, the soil potential at (and above) which stomates are fully open (ψ_o) and the value at which stomates are fully closed (ψ_c).

$$f_{w,\text{SMS}} = \sum_{i=1}^{n} r_i w_i \qquad (3)$$

$$w_i = 0 \le \frac{\psi_{\text{soil},i} - \psi_c}{\psi_o - \psi_c} \le 1 \qquad (4)$$

2.4.2 SMS Root Water Uptake

The CLM features a vertically discretized soil column with variable soil layer thicknesses. The number of soil layers (n) can vary, depending on the depth to bedrock. Soil water movement in each soil layer is governed by Richards' equation, with root water uptake (q_i) incorporated as a sink term. Summed over the soil column, root water uptake is required to equal transpiration (T).

$$T = \sum_{i}^{n} q_i \qquad (5)$$

In the SMS configuration, a heuristic function (based on $f_{w,\text{SMS}}$) is used to determine q_i. Transpiration is partitioned among the soil layers based on the product of the root fraction and the wilting factor, which is then normalized by f_w to satisfy Equation 5.

$$q_i = \frac{r_i w_i}{f_w} T \qquad (6)$$

196   Substituting for w_i yields the SMS root water uptake equation as a function of the
197 layer-i soil potential ($\psi_{\mathrm{soil},i}$).

198
$$
q_i = \begin{cases} 0 & \text{if } \psi_{\mathrm{soil},i} < \psi_c \\[2ex] \dfrac{T}{f_w} \dfrac{r_i}{\psi_o - \psi_c} \left(\psi_{\mathrm{soil},i} - \psi_c \right) & \text{if } \psi_c \leq \psi_{\mathrm{soil},i} \leq \psi_o \\[2ex] \dfrac{T}{f_w} r_i & \text{if } \psi_{\mathrm{soil},i} > \psi_o \end{cases}
\tag{7}
$$

199   In the Darcy framework, water fluxes are the product of hydraulic conductance (k_i) and
200 hydraulic gradient ($\Delta\psi$). Although SMS does not explicitly calculate hydraulic conductance,
201 Equation 7 can be used to define hydraulic analogs resulting from the transpiration partition-
202 ing heuristic function, allowing easier comparison to the PHS root water uptake implementa-
203 tion.

204
$$
\begin{aligned}
q_i &= -k_i \Delta\psi \\
\Delta\psi &= \psi_c - \psi_{\mathrm{soil},i} \\
k_i &= \frac{T}{f_w} \frac{r_i}{\psi_o - \psi_c}
\end{aligned}
\tag{8}
$$
$$
\text{constrained by:} \quad \Delta\psi = \begin{cases} 0 & \text{if } \psi_{\mathrm{soil},i} < \psi_c \\ \psi_c - \psi_o & \text{if } \psi_{\mathrm{soil},i} > \psi_o \end{cases}
$$

2.5 PHS (CLM5 default)

205

2.5.1 PHS Water stress factor

206

207   PHS introduces a new formulation of the water stress function, f_w, which is based on
208 leaf water potential (ψ_{leaf}) instead of soil potential (described further in Section 2.5.5). The
209 relationship is modeled with a sigmoidal function, subject to two parameters: the water po-
210 tential at 50% loss of stomatal conductance (ψ_{50}) and a shape-fitting parameter (c_k).

211
$$
f_{w,\mathrm{PHS}} = 2^{-\left(\frac{\psi_{\mathrm{leaf}}}{\psi_{50}} \right)^{c_k}}
\tag{9}
$$

212   Utilizing leaf water potential, instead of soil water potential, for drought stress intro-
213 duces a new interpretation of vegetation water stress to the model. Leaf water potential is
214 modulated by supply of sap to the leaves and by evaporative demand, as regulated by stom-
215 atal dynamics [*Novick et al.*, 2016b]. As a result, low soil water (bottom-up stress) induces
216 stress due to limited water supply, but in addition, high atmospheric VPD can induce stress
217 with the associated increases in the gradient in water potential across the plant xylem (top-
218 down stress). This latter mechanism was absent from the previous water stress function (de-
219 pendent on soil water potential only), by construction. Given the observed increase in VPD
220 with global warming, it appears critical to include such mechanistic dependence of water
221 stress. While the Medlyn stomatal conductance model does depend on VPD, the model does
222 not (given constant g_1) reflect the risk of hydraulic failure [*Zhou et al.*, 2013]. The new stress
223 factor formulation reflects the dual risks of soil moisture deficit and atmospheric demand on
224 hydraulic safety [*Williams et al.*, 2013], requiring vegetation to avoid excessive xylem tension
225 associated with risk of cavitation.

2.5.2 PHS Root Water Uptake

PHS implements an alternative to the SMS heuristic approach for root water uptake, using a mechanistic representation following Darcy's Law. Instead of a constant parameter (ψ_c) defining $\Delta\psi$, PHS implements a physical model of vegetation water potential (described in Section 2.5.3). The water flux from a given soil layer is driven by the gradient between soil potential ($\psi_{\mathrm{soil},i}$) and the water potential in the root collar (ψ_{root}), after accounting for the effects of gravity ($\rho g z_i$, where z_i is the soil layer depth). Hydraulic conductance across the soil and roots (k_{sr}) is modeled based on soil hydraulic properties and xylem vulnerability, accounting for both the path across the soil matrix and through the xylem conduits (details in Appendix B).

$$q_i = -k_{sr,i}\left(\psi_{\mathrm{root}} - \psi_{\mathrm{soil},i} + \rho g z_i\right) \tag{10}$$

2.5.3 Modeling Vegetation Water Potential

The PHS model within CLM5 uses Darcy's law to model the flow of water through the SPAC, which can be represented with an electrical circuit analogy (Figure 1). PHS solves for vegetation water potential along the path from soil-to-atmosphere. Vegetation water supply and demand are both coupled to vegetation water potential, as described in the previous two sections. The solution for vegetation water potential is the set of values that matches supply with demand, maintaining water balance across each of the vegetation water potential nodes.
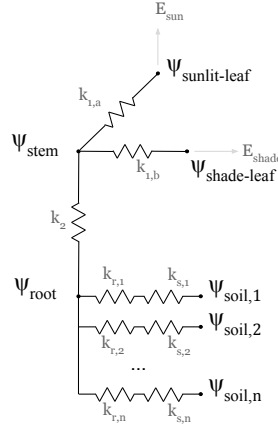
Figure 1. Plant hydraulic circuit analog schematic

PHS solves for vegetation water potential at four locations: ψ_{root}, ψ_{stem}, $\psi_{\mathrm{shade-leaf}}$, and $\psi_{\mathrm{sun-leaf}}$. The number of nodes is chosen as the strict minimum to allow for differences in segment parameterizations [*Simonin et al.*, 2015; *Sperry and Love*, 2015], while also conforming to existing CLM model structure (vertically discretized soil layers, 2-big-leaf). At each node in the circuit diagram (Figure 1), we model water potential, and, between nodes, we resolve the flux of water based on Darcy's law. Water uptake from the different soil layers is assumed to operate in parallel; a typical assumption justified by higher resistance in lateral versus central roots (e.g. *Williams et al.* [2001]). Two resistors operate in series between each ψ_{soil} and ψ_{root}, to represent the path across the soil matrix and then through the root tissue [*Williams et al.*, 1996]. Specifics on the parameterization of hydraulic conductance for each segment are provided in Appendix B.1. Solving for vegetation water potential requires matching vegetation water supply (root water uptake, sap flux through the stem) with vegetation water demand (sunlit and shaded leaf transpiration).

2.5.4 Water supply

Water supply is modeled via Darcy's Law, where flux of water (q) is the product of the path hydraulic conductance (k) and the gradient in water potential ($\psi_2 - \psi_1$) after accounting for gravitational potential ($\rho g \Delta z$). Equation 11 represents the flow from a generic node 1 to node 2.

$$q = -k\left(\psi_2 - \psi_1 + \rho g \Delta z\right) \tag{11}$$

For simplicity, PHS does not represent plant tissue water storage (or capacitance, using the electrical circuit analogy), which is in line with recent supply-loss theory [*Sperry and Love*, 2015]. Capacitance significantly complicates the water potential solution [*Celia et al.*, 1990] and is challenging to parameterize [*Bartlett et al.*, 2016]. However, buffering of water stress provided by tissue water storage could potentially be important especially on sub-daily timescales [*Meinzer et al.*, 2009; *Epila et al.*, 2017], whereby its inclusion may be warranted in future model versions.

Hydraulic conductance through vegetation segments is modeled following empirical xylem vulnerability curves [*Tyree and Sperry*, 1989], where segments lose conductance with increasing xylem tension related to cavitation and embolism [*Holbrook et al.*, 2001]. The vulnerability curves model loss of conductance relative to maximum conductance ($k_{\max}$) using two parameters: c_k, a sigmoidal shape-fitting parameter, and p_{50}, the water potential at 50% loss of segment conductance (following *Gentine et al.* [2016]).

$$k = k_{\max} \, 2^{-\left(\frac{\psi_1}{p_{50}}\right)^{c_k}} \tag{12}$$

Both c_k and p_{50} can be estimated from field experiments [*Sack et al.*, 2002], and p_{50} is available in the TRY trait database [*Kattge et al.*, 2011]. Parameterization based on p_{50} aligns with the call for a transition to models that use a wider range of plant functional trait data in their parameterization [*Anderegg*, 2015a]. The loss of xylem conductivity is based on lower terminal water potential (ψ_1) as is typical in other simplified models [*Xu et al.*, 2016], but may underestimate the integrated loss of conductivity [*Sperry and Love*, 2015].

PHS models root, stem, and leaf tissue conductances according to equation 12. The parameterization of $k_{\max}$ varies by hydraulic segment (see details in Appendix B1). The conductances across the soil matrix ($k_{s,1},...,k_{s,n}$) to the root surface follows *Williams et al.* [2001] and *Bonan et al.* [2014], which scales soil conductivity [*Brooks and Corey*, 1964; *Clapp and Hornberger*, 1978] by an appropriate conducting distance based on the root distribution. Details are provided in Appendix B1.

2.5.5 Water demand

Water demand is calculated using the Medlyn stomatal conductance model (see Section 2.1) modulated by the CLM water stress factor. As discussed earlier f_w is based on leaf water potential in PHS, where stress increases as leaf water potential becomes more negative [*Klein and Niu*, 2014]. Because leaf water potential is modeled separately for sunlit and shaded leaves, f_w takes on distinct sunlit and shaded values.

$$
\begin{aligned}
f_{w,sun} &= 2^{-\left(\frac{\psi_{\text{sun-leaf}}}{\psi_{50}}\right)^{c_k}} \\
f_{w,shade} &= 2^{-\left(\frac{\psi_{\text{shade-leaf}}}{\psi_{50}}\right)^{c_k}}
\end{aligned}
\tag{13}
$$

Shaded and sunlit leaf transpiration (E_{sun}, E_{shade}) are calculated by attenuating maximal transpiration ($E_{\text{sun,max}}$, $E_{\text{shade,max}}$) according to f_w. $E_{\text{sun,max}}$ and $E_{\text{shade,max}}$ are calculated at the beginning of each timestep by running the stomatal conductance model with $f_w = 1$. Equations (13) and (14) reflect a simplification used within iterations of the PHS module, neglecting non-linear components of the relationship between stress and transpiration (described further in Section zqz).

$$
\begin{aligned}
E_{\text{sun}} &= f_w E_{\text{sun,max}} \\
E_{\text{shade}} &= f_w E_{\text{shade,max}}
\end{aligned}
\tag{14}
$$

2.5.6 PHS solution

PHS solves for the set of vegetation water potential values (ψ) that matches water supply (root water uptake) to water demand (transpiration), while satisfying continuity across the four water flow segments (soil-to-root, root-to-stem, stem-to-leaf, and leaves-to-transpiration). Beginning from an initial condition of ψ (from the previous timestep), PHS computes the flux divergence f (representing the mismatch of flow in and out of each segment) and iteratively updates ψ until it reaches convergence, i.e. $f \rightarrow 0$.

$$
\psi = \begin{bmatrix} \psi_{\text{sun}} \\ \psi_{\text{shade}} \\ \psi_{\text{stem}} \\ \psi_{\text{root}} \end{bmatrix}
\tag{15}
$$

$$
f(\psi) = \begin{bmatrix} E_{sun} - q_{sun} \\ E_{shade} - q_{shade} \\ q_{sun} + q_{shade} - q_{stem} \\ q_{stem} - \sum_{j=1}^{n} q_{root,j} \end{bmatrix}
\tag{16}
$$

$$
A = \frac{df}{d\psi}
\tag{17}
$$

While $|f| > 0$

$$
\begin{aligned}
\Delta\psi &= A^{-1} f(\psi_i) \\
\psi_{i+1} &= \psi_i + \Delta\psi
\end{aligned}
\tag{18}
$$

The numerics are tractable because f has continuous, analytical derivatives and A (a 4x4 matrix with six null entries) is easy to invert when well-conditioned. Supply and demand converge, because transpiration demand decreases with more negative leaf water potentials and supply increases with more negative leaf water potentials. The PHS loop is nested within iterations for intercellular CO_2 concentration and leaf temperature. The non-linear relationship between f_w and transpiration is resolved through iteration for converging f_w alongside intercellular CO_2. Details on the numerical implementation are provided in Appendix Section B.1.

3 Experiment Description

We use a set of four simulations to assess the impact of the plant hydrodynamics model (PHS versus SMS) on a tropical rainforest site, under ambient conditions and partial precipitation throughfall exclusion. This site is located in Eastern Amazonia (Caxiuanã, Brazil) and part of the Large-Scale Biosphere-Atmosphere Experiment in the Amazon [*Avissar et al.*, 2002].

1. SMS, with ambient precipitation throughfall (AMB)

Table 1. Select parameter values

CLM name	Full Name	Symbol	Value
kmax(1)	Maximum Sun Branch Conductance	$k_{sun,max}$	4e-8 s^{-1}
kmax(2)	Maximum Shade Branch Conductance	$k_{shade,max}$	4e-8 s^{-1}
kmax(3)	Maximum Stem Conductivity	$k_{stem,max}$	4e-8 m/s
krmax	Maximum Root Conductivity	$k_{r,max}$	6e-9 m/s
psi50	Water potential at 50% loss of conductivity	ψ_{50}	-1.75 MPa
ck	Vulnerability shape parameter	c_k	2.95
smpso	Soil potential with stomata fully open	ψ_o	-0.65 MPa
smpsc	Soil potential with stomata fully closed	ψ_c	-2.5 MPa
medlyn_intercept	Medlyn intercept	g_0	100 μmol / m2 / s
medlyn_slope	Medlyn slope	g_1	6 kPa$^{0.5}$
n	Soil porosity to 4.64 meters	n	0.42
n	Soil porosity beyond 4.64 meters	n	0.28
hksat	Saturated soil hydraulic conductivity	$k_{s,max}$	3e-5 m/s
sucsat	Saturated soil matric potential	ψ_{sat}	461 Pa
bsw	Brooks-Corey parameter	b	6

2. SMS, with 60% of precipitation throughfall excluded (TFE)

3. PHS, AMB

4. PHS, TFE

All four simulations use the same version of CLM5 (development version r270, www.github.com/ESCOMP/ctsm/releases/t which features a switch that can toggle between SMS and PHS configurations. Simulations are run offline (uncoupled from an active atmospheric model), spanning from 2001 through 2003, utilizing the satellite phenology (SP) mode of CLM5 in which vegetation state (LAI, canopy height) is prescribed and biogeochemistry is inactive. Six-year spin-up simulations (one each for SMS and PHS) are used to create initial conditions, repeating the Ambient simulation twice. Descriptions of site characteristics, forcing data, and observational sap flux and soil moisture, can be found in *Fisher et al.* [2007] and *Fisher et al.* [2008].

3.1 Parameter Values and Throughfall Exclusion

Parameter values concerning vegetation hydrodynamics are presented in Table 1. All other parameters use the default values associated with the r270 version of CLM5. Informed by parameter values reported in *Fisher et al.* [2008], we tuned soil hydraulic parameters and the throughfall exclusion rate, to improve simulated soil moisture relative to observations (Supp Fig A.9). A 972-member ensemble of simulations was used to tune the parameters for the PHS configuration to reasonably reflect sap flux observations (see Appendix B.4).

4 Results

4.1 Comparison with observations

We tested two configurations of CLM5 with simulations of the Caxiuanã throughfall exclusion experiment over 2002-2004. We compare modeled transpiration with observations derived from sap flux velocity and modeled soil moisture with observations using TDR sensors (see above for experiment and observation details).
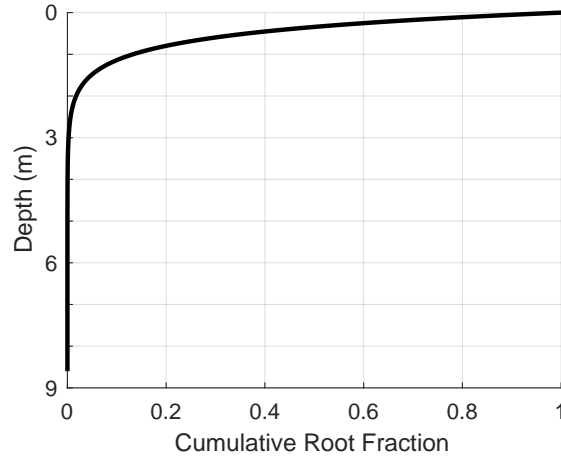
Figure 2. Cumulative rooting distribution

4.1.1 Transpiration, Ambient Conditions

Under ambient conditions, PHS reduces error and improves correlation between modeled and observed transpiration (compared to SMS, Figure 3a,c). While the two models make a similar number of small errors, SMS commits more errors exceeding 1 mm/day. The absolute value of SMS-OBS transpiration (Figure 4g) exceeds 1 mm/d in 67 of 414 days with available observations, as compared to just 23 with PHS. And while PHS error is limited to a maximum of 1.6 mm/d, SMS error exceeds 2 mm/d twelve times (all of which underestimate transpiration relative to observations). The largest SMS errors coincide with dry soils, which is discussed further in Section zqz.

While PHS offers improvements modeling transpiration as measured by RMSE and correlation, the ambient simulation seems to underestimate transpiration variability, with a standard deviation of daily transpiration of 0.61 mm/d compared to 0.87 mm/d in the observations (with SMS, the standard deviation is 0.97 mm/d). As such, PHS features a low bias for high transpiration values and a high bias for low transpiration values (Figure 3c). The difference in modeled transpiration between PHS and SMS derives from divergent water stress dynamics, which are discussed in Section zqz.

4.1.2 Transpiration, TFE

Both models have a harder time modeling transpiration under TFE, with higher RMSE and lower correlation to observations as compared to the ambient simulations (Figure 3b,d). PHS performs better than SMS, but yields a more pronounced high bias (Figure 3b,d). The wet season (February-March-April), especially, is prone to high transpiration biases in both models, where, in the observations, transpiration is reduced 32% by TFE, as compared to modeled reductions of only 1.6 and 4% for PHS and SMS, respectively. This may indicate that the models' sensitivity to soil potential declines are underestimated, or that water drains from the root zone more quickly after precipitation events than we represent in these simulations (Figure 5b,d). Difficulty reproducing the effect of TFE (and the influence of soil moisture on leaf gas exchange) at Caxiuanã has precedent in the literature [*Restrepo-Coupe et al.*, 2017; *Powell et al.*, 2013].

4.1.3 Soil Moisture

The second source of observations for model evaluation is volumetric soil moisture. These data are used to evaluate the parameterization of root water uptake, which is updated with PHS. Modeled soil moisture values (at a depth of 50 cm) are comparable between model configurations during the wet season (February-March-April) under ambient conditions, both yielding averages of 28% (Figure 5a,c). With excess rainfall, soil moisture is largely determined by the soil field capacity and saturated conductivity, which are the same in both model configurations. With water shortfalls, the root water uptake parameterizations drive the soil moisture dynamics, and the models diverge, as SMS consistently generates lower soil moisture values (than PHS) within the first meter of the soil column (Figure 5, Supp Fig A.10). Soil moisture averages to 10% during the dry season (September-October-November, ambient case, depth=50cm) with SMS, as compared to 16% with PHS. PHS better comports with observations, reducing RMSE by 57% relative to SMS (Figure 5a,c).

We highlight the soil moisture at 50 cm depth, but similar patterns are observed throughout the first meter of the soil column (Supp Fig A.10). The 50-cm depth emphasizes the effect of modeled root water uptake, because it features higher root fraction than the deeper soil layers (Figure 2), but avoids the high frequency dynamics of the top soil layer from soil evaporation and precipitation events that do not relate to differences between PHS and SMS. Under TFE, SMS minimum soil moisture is again limited to 10%, but holds there for a longer duration (Figure 5). Contrastingly, PHS achieves lower dry season soil moisture values under TFE as compared to ambient conditions. PHS better comports with observations, reducing RMSE by 42% relative to SMS (Figure 5a,c), however both models seem to feature a high bias in soil moisture in the root-zone (under TFE) during the wet season (Figure 5, Supp Fig A.10).

4.2 Vegetation water potential

PHS updates both the water stress and root water uptake parameterizations based on modeling vegetation water potential. Leaf water potential features a pronounced diurnal cycle, reaching -1.65 MPa at midday (Figure 6a). Most of the midday pressure drop occurs between ψ_{root} and ψ_{stem} (Δ=-1.47 MPa), representing the root collar and upper stem, respectively. Stem, shade, and leaf curves are all roughly equal, resulting in overlapping lines in Figure 6a, relating to high stem-to-leaf conductance from the parameter values used in this experiment. Stem-to-leaf conductance does not drive leaf water potential in the current parameterization of the model, but may be important to investigate further, given the reported dynamics of leaf conductance [*Simonin et al.*, 2015].

Under TFE, model midday leaf water potential decreases to -2.31 MPa (Figure 6b). This change derives from a decrease in predawn root water potential (lower soil moisture) and in the drop in root water potential between predawn and midday (due to reduced soil-to-root conductance). This comports with previous evidence that seasonal changes in hydraulic resistance are larger belowground [*Fisher et al.*, 2006]. Despite reduced stem conductance, the pressure drop from root-to-stem acts in the opposite direction, reduced in magnitude to -1.02 MPa (from -1.47 MPa), following from 54% reductions in transpiration. In this way, stomatal regulation serves to mitigate the drop in leaf water potential due to soil drying and reduced hydraulic conductance.

Midday leaf water potential features a seasonal cycle, with lower values during the dry season (Figure 6c). Under ambient conditions, modeled root water potential values match wet season observations, but are less negative than dry season observations [*Fisher et al.*, 2006]. Modeled leaf water potential values under ambient conditions are less negative than field observations (*Fisher et al.* [2006] report average ψ_{leaf} of -1.71 MPa during the wet season and -2.47 MPa during the dry season), but are within the range of observations. The parameter values used here may underestimate isohydricity (which would be reflected by minimal leaf water potential drop during drought) in response to TFE, given that observa-

Table 2. Root-zone soil potential ^{a} (MPa) terciles. The two cut-points are used to divide the points in each subplot of Figure 8 into three groups, based on root-zone soil moisture.

Simulation	T1	T2
SMS, Ambient	-0.01	-0.54
SMS, TFE	-0.29	-1.74
PHS, Ambient	-0.01	-0.05
PHS, TFE	-0.05	-0.33

^{a}SMS values correspond to daily mean root-fraction weighted soil potential.
PHS values correspond to predawn root water potential.

tions showed no significant difference between ambient and TFE leaf water potential [*Fisher et al.*, 2006].

4.3 Stress dynamics

Modeling vegetation water potential enables a diurnal mode of variability in vegetation water stress. While the SMS stress factor has minimal diurnal variability, PHS features increased stress at midday (Figure 7a,b), corresponding to the drop in leaf water potential induced by increasing demand for transpiration (Figure 6b,c). Average midday stress values are comparable between the two model configurations during the 2003 dry season (Figure 7), but PHS achieves more photosynthesis over the course of the average dry-season day (Supp Fig A.2), due to lower stress in the mornings and afternoons.

The SMS stress factor lacks diurnal variability, because it is based on average root-zone soil matric potential (Equation 3), which evolves over longer timescales. PHS utilizes leaf water potential to calculate stress (Equation 9), which responds to both water supply and transpiration demand. As such, the PHS stress factor responds to both soil moisture and VPD, while SMS responds only to soil moisture (Figure 8). Under ambient conditions, SMS features significant stress associated with declining soil water status, but PHS stress is primarily demand-driven, with less impact from soil moisture (Figure 8a,c). With TFE, stress increases in both model configurations, and the effect of soil moisture on PHS stress increases markedly (Figure 8d).

4.4 GPP

The two stress parameterizations feature differing seasonal cycles, with PHS experiencing less seasonal variability in stress (Figure 9a-d). Under ambient conditions, SMS predicts little to no stress (f_w=1) during the wetter months (January through July). Meanwhile PHS models significant stress, with highly variable f_w, ranging as low as 0.5. Despite abundant soil water, PHS still imposes stress, due to high transpiration demand when VPD and downwelling solar radiation are high. This results in lower wet season GPP than with SMS (Figure 9e,g). Contrastingly, SMS imposes more stress than PHS during the dry season (Figure 9b,d), resulting in lower dry season GPP. Observations show increased GPP during the dry season [*Restrepo-Coupe et al.*, 2017], suggesting that both model configurations, but especially SMS, may overestimate dry season water stress under ambient conditions.

The modeled effect of TFE is relatively small during the wet season, with modeled reductions in GPP of 1.3 and 3.8% for PHS and SMS, respectively. Based on transpiration observations, both configurations likely underestimate the TFE effect during the wet season (discussed further in Section zqz). SMS imposes more dry season stress, resulting in a 63% reduction of GPP due to TFE, compared to 44% with PHS. Comparing dry season stress to the wet season, and TFE conditions to ambient, precipitation shortfalls (and the associate

reductions in soil moisture) lead to less added stress under PHS as compared to SMS. How-
ever, PHS experiences more stress overall, due to the effects of xylem tension imposed by the
gradient of water potential from soil-to-leaf (discussed further in Section zqz).

4.5 Root water uptake (RWU)

In addition to updating water stress, PHS implements updated RWU, consistent with
hydraulic theory. The parameterization of RWU affects the vertical distribution of soil wa-
ter (Figure 10, Supp Fig A.9), as SMS tends to achieve drier upper soil layers, whereas PHS
spreads the drying effects of transpiration over a larger vertical extent. As described in Sec-
tion zqz (Figure 5), this yields a dry bias relative to soil moisture observations in the root-
zone for SMS (within the dry season).

RWU is the product of hydraulic conductance ($k_{s,r}$) for water flow and the gradient
($\Delta\psi$) in water potential from $\psi_{\text{soil},i}$ to ψ_{root} (see Section zqz). With PHS, reductions in RWU
with drying are imposed by declining conductance. On the other hand, $\Delta\psi$ tends to increase
with drying (due to dynamic ψ_{root}), partially mitigating the reduction of RWU. PHS exhibits
high sensitivity to soil potential, because $k_{s,r}$ falls off by almost 3 orders of magnitude as soil
potential declines from 0 to -1 MPa (Supp Fig A.6). This derives mostly from the exponen-
tial dynamics of soil conductivity [*Brooks and Corey*, 1964]. With SMS, the opposite is true:
reductions in RWU are imposed by declining hydraulic gradient (as soil potential approaches
the constant ψ_c, -2.5MPa) and are (to a small extent) mitigated by increases in the (implied)
conductance. As a result, RWU (within a given soil layer) is more sensitive to soil potential
with PHS (Figure 11), which prevents soil potential from getting much lower than -1 MPa, as
compared to values as low as -2.5MPa under SMS.

While RWU within a given soil layer is more sensitive to soil potential with PHS, tran-
spiration overall is less sensitive to shortfalls in precipitation (as compared to SMS) associ-
ated with dry season onset and TFE (Figure 4). This is because, within PHS, there is more
flexibility to compensate for dry layers by switching the RWU to moist layers. As such, PHS
can compensate for the sensitivity to soil potential by spreading the drying associated with
the transpiration sink over a larger vertical extent (Figure 10). Following from this, with
PHS, dry season transpiration is less sensitive to TFE, due to increased RWU from below
2 meters in depth (Figure 12d). The shifting of water extraction based on water availability is
also present under ambient conditions, as PHS shifts RWU from near-surface (0-0.2m depth)
to the deeper soil layers (beyond 0.2m) during drydowns (Figure 12a-c).

Finally I could point out non-linearity in (Supp Fig A.6) to explain why SMS ψ_s gets
stuck at ψ_c.

4.6 Hydraulic redistribution

SMS precludes hydraulic redistribution (HR) setting root water uptake to zero when re-
versed gradients in water potential occur (contrary to PHS). With PHS, HR totals to 38.9 cm
under ambient conditions and 40.0 cm under TFE over the course of 2003, with the major-
ity (28.0, 26.7 cm) of this HR occurring at night (Figure 13). in line with established theory
[*Jackson et al.*, 2000]. HR occurs in both directions (Supp Fig A.8), but is predominately
downwards (AMB: 30.7cm, TFE: 33.8cm). The amount of HR is difficult to constrain due to
scarce observations. The simplicity of the hydraulic representation may lead to overestimat-
ing HR, which is discussed further in Section zqz.

4.7 Soil moisture effect on transpiration

Model soil potential shows limited relationship to sap flux observations under ambient
conditions (Supp Fig A.11b,f), which is indicative of limited soil moisture stress. However,

in the SMS configuration, modeled transpiration decreases strongly with more negative soil potential (Supp Fig A.11a), biasing the model relative to observations (Fig 14a).

Sap flux observations under TFE show a stronger relationship with soil potential especially with PHS (Supp Fig A.11h,d). With SMS, the modeled attenuation of transpiration with soil potential again seems to bias modeled transpiration (Fig 14b). Derived from ψ_c, transpiration approaches zero when soil potential reaches -2.5 MPa (Supp Fig A.11c). The two PHS simulations feature less structure in transpiration bias vs. soil potential and less bias overall (Fig 14c,d).

5 Discussion

5.1 Can modeling vegetation water potential improve the CLM?

In this study, we have implemented plant hydraulic theory within CLM5, using dynamic vegetation water potential to modulate leaf gas exchange and root water uptake. PHS installs a model for predicting vegetation water potential by extending Darcy's Law through the vegetation substrate (Figure 1), creating four new water potential prognostic variables (ψ_{root}, ψ_{stem}, $\psi_{\text{shade-leaf}}$, and $\psi_{\text{sun-leaf}}$). The model is able to capture expected diurnal and seasonal dynamics of vegetation water potential, with lower values within the stem and leaves at midday and during the dry season (Figure 6). PHS uses the new vegetation water potential variables to advance the physical basis for representing the SPAC, particularly with regard to modeling vegetation water stress and root water uptake.

To demonstrate the new model dynamics, we utilized a site-level experiment testing PHS by simulating the Caxiuanã throughfall exclusion experiment [*Fisher et al.*, 2007]. We found that PHS improves output for both transpiration and soil moisture relative to observations as compared to the control model (see Section 4.1, Figures 3,5). While this is encouraging, especially given the nature of the previous bias (see Section zqz), the improvement is specific to the site and experiment described herein, and model skill will need to be reevaluated in a broader context. Instead, the value of opting for a single site (in lieu of global simulations) resides in the opportunity to perform the detailed analyses to elucidate the new model dynamics in order to complement this first description of PHS.

5.2 Stomatal conductance: Soil moisture stress vs. Xylem tension stress

The first of these analyses is of the response of stomatal conductance stress to environmental factors, namely: soil moisture, vapor pressure deficit, and solar radiation. The Medlyn stomatal conductance model, as implemented in the CLM, requires a notion of water stress to attenuate stomatal conductance in order to capture the effects of diminishing water supply, with various relevant implementations described in the literature (see Section zqz). We tested two such approaches, which alternatively base stress on either soil water potential (SMS) or leaf water potential (PHS). The two configurations feature significantly different stress dynamics on both diurnal and seasonal timescales (Figures 7,9).

Leaf water potential is (in simplified terms) the sum of soil water potential and the gradient of water potential from soil-to-leaf ($\psi_l = \psi_s + \Delta\psi$). Therefore using ψ_l as the driver of water stress preserves a relationship between stress and soil potential, but now also represents the effect of increasing demand for transpiration (reflected by increases in $\Delta\psi$) on water stress, through increased xylem tension. As such, PHS offers a mechanistic approach to water stress, utilizing a physical justification that interprets water stress as the result of increasing xylem tension, which has previously been used as a primary [*Sperry et al.*, 2017] or contributing [*Novick et al.*, 2016b] factor to stomatal regulation. In the model, vegetation will (according to the specific hydraulic parameter values) limit transpiration in order to avoid cavitation and embolism associated with overly negative water potentials. As a result, PHS stress responds to changing soil moisture, but unlike SMS, also responds to VPD and

downwelling solar radiation (Figure 8), which modulate transpiration demand. This imparts a diurnal pattern to PHS stress, with higher stress around midday, whereas with SMS, stress is relatively constant throughout the day (Figure 7).

Soil water potential approaches (as in SMS) lack a straightforward physical basis, but rather empirically relate stomatal conductance and/or photosynthetic parameters with soil potential (or soil moisture). However, in the case of SMS, the empirical relationship is very difficult to constrain, due to scarce observations of the stress driver, root-fraction-weighted soil potential. As a result, soil moisture stress functions have been shown to contribute significant uncertainty to the carbon cycle in Earth System Models [*Trugman et al.*, 2018]. Leaf water potential, on the other hand, is more easily measured in situ [*Boyer*, 1967], and has been shown to correlate with remote sensing products [*Momen et al.*, 2017], offering better observational constraints for PHS.

Another key difference is that PHS stress imparts a negative feedback on GPP and transpiration. Conditions favoring increased GPP (e.g. more light) also increase transpiration demand, leading to more xylem tension and stress, which opposes increases in GPP. In the PHS simulations, this suppresses variability in GPP relative to SMS, and leads to underestimating the range of transpiration compared to sap flux observations (Figure 3). Terrestrial biosphere models have previously had difficulty reproducing variability observed in GPP [*Keenan et al.*, 2012], and evaluating the change in variability introduced by PHS will be an important follow-up to this study. With PHS, the relative contributions (to water stress) of changes in transpiration demand versus changes in soil potential (and likewise the strength of the negative feedback described above) can be varied by adjusting the hydraulic parameters. This establishes a flexible representation of vegetation water use dynamics that can be used to test hypotheses about drought resilience, water use strategies, and the relative impacts of soil moisture and VPD on stress.

5.3 Structural improvements in modeling root water uptake

5.3.1 Dynamic vegetation water potential

PHS introduces dynamic vegetation water potential, for the first time, into the default configuration of the CLM. Seasonally and diurnally dynamic leaf water potential are observed in the field [*Fisher et al.*, 2006], adjusting to variations in soil water supply and transpiration demand. The dynamism in the gradient of water potential from soil-to-leaf, according to Darcy's Law, should drive RWU [*Jarvis*, 2011]. A mechanistic representation of this process is important for modeling the range of water use strategies, and/or testing hypotheses regarding these on the ESM scale, such as the effects of iso/anisohydry on leaf gas exchange and drought vulnerability.

5.3.2 Mechanistic hydraulic conductance, with response to drying

Likewise, PHS implements mechanistic hydraulic conductance through the SPAC, reflecting declines in conductance associated with decreasing water potential in both plant vessels and soil substrate [*Tyree and Sperry*, 1989]. Hydraulic theory describes soil conductance as featuring an exponential relationship with soil potential [*Brooks and Corey*, 1964], ranging three orders of magnitude over the range of soil potential observed in our simulations. This shapes the PHS response of RWU to soil drought, and is not captured by the linear loss of RWU exhibited in SMS (between the parameters: ψ_o and ψ_c, Figure 11). As a result, PHS RWU is more sensitive to drying soils, which seems to ameliorate dry biases in soil moisture observed in SMS relative to observations (Figure 5)

5.3.3 Compensatory RWU

- Furthermore utilziing hydraulic approach enables compensatory root water uptake.

- where, for example, as surface soil layers dry, tap roots can be used to harness reserves of soil water at depth [*Oliveira et al.*, 2005] to compensate for reduced RWU near the surface and maintain transpiration and photosynthesis.
- This is a known shortcoming of the SMS-style transpiration sink [*Jarvis*, 2011].
- For example, PHS extracts 29% of transpiration from beyond 2 meters depth under TFE (during the 2003 dry season) as compared to 13% with SMS.
- In PHS, as the surface soil layers dry out, conductance decreases rapidly, leading to reduced RWU.
- In response, the vegetation 'pulls' harder, lowering ψ_{root}, creating a larger gradient to the deeper soil layers, yielding increased RWU in the still-moist layers.
- Due to constant vegetation potential (ψ_c) and no drying response to conductance, SMS lacks the flexibility to achieve this type of CRWU.

5.3.4 Hydraulic redistribution

PHS simulates substantial HR at our test site, both upwards and downwards (Figure 13, Supp Fig A.8), which conforms with field observations [*Burgess et al.*, 1998; *Oliveira et al.*, 2005]. Modeled HR is weighted towards downward transfers, moving near-surface water from rain events deeper into the soil column and thus saving it for when it is most needed such as during the dry season. This would seem to convey an advantage to deep-rooted individuals, banking water for later use out of reach of shallow-rooted competitors. HR can offer significant water subsidies during dry periods [*Jackson et al.*, 2000] and has been highlighted as an important missing feature in CLM [*Lee et al.*, 2005]. However, we should note that observations of HR are extremely difficult and rare, and the degree to which HR actually occurs in real-world systems remains unclear. Unequivocal detection of HR involves the observation of reverse flow along transport roots, typically at rates close to the detection threshold of sap flow monitoring systems.

Installing a representation of HR was not a primary objective in the development of PHS. Rather it was the natural consequence of our simplified Darcy's Law implementation for root water uptake. However, it remains to be seen whether HR, as modeled in this implementation, is a feature or a liability. One challenge we faced was that in an initial implementation of PHS, HR seemed to oversupply the top layer of the soil column (spanning 0 to 2 cm below the ground surface) and thus significantly degraded modeled soil evaporation (not shown). To remedy this problem, we set the hydraulic conductance to zero in the uppermost soil layer, disallowing any root water uptake there.

PHS may overestimate HR, given the simplified root system architecture [*Bouda and Saiers*, 2017] and the lack of an explicit representation of fine-root cavitation [*Kotowska et al.*, 2015]. In our simulations, HR increases annual total root water uptake by up to 52% relative to transpiration alone (2003, TFE). Other models, similar to the SMS paradigm, disallow HR by constraining root water uptake to be positive [*Xu et al.*, 2016]. We view the PHS implementation of HR into the default versions of the CLM as a 'null' hypothesis for the functioning of this process, and as a platform to allow further refinement from the plant hydraulics community. Isotopologues of water could be used as a tool to further constrain this redistribution in the CLM in the future.

5.3.5 No-brainers

- absolute roots
- penalties
- ditch the ψ_o constraint

5.3.6 *Influence on soil moisture dynamics and transpiration*

5.4 Soil moisture dynamics

Partly due to HR, vertical and temporal gradients in soil water potential are significantly reduced in PHS (Figure 10). This can also be attributed to the root water extraction hydraulic gradient ($\Delta\psi$), which is significantly smaller in PHS (Supp Fig A.7). In turn, SMS features a significant dry bias relative to soil moisture observations, especially in the first meter of the soil column. This indicates that SMS root water uptake is 'pulling' too hard, and that ψ_c is too low, at least regarding soil moisture dynamics. PHS reduces soil moisture RMSE by up to 55% relative to SMS (Figure 10).

In the literature, ψ_c is primarily associated with its role governing the response of transpiration and photosynthesis to soil moisture [*Powell et al.*, 2013; *Bonan et al.*, 2014; *Rogers et al.*, 2017]. We show that it likewise has significant control over soil moisture, itself. Throughout the four simulations, ψ_c (equals -2.5MPa) is significantly lower than ψ_{root}, yielding a larger hydraulic gradient, and the dry bias in soil moisture. Likewise, during dry periods, soil potential has a tendency to take on the specific value of ψ_c over significant areas of space/time. Constrained to the top 2 meters of the soil column (which contains 98% of the total root fraction, Figure 2), 38.9% of the space-time area in Figure 10a is within 0.1 MPa of ψ_c. This can occur even without TFE, where Soil Layer 8 (spanning 68 to 92cm below ground) spends 23.2% of the time during 2003 within 0.1 MPa of ψ_c (Supp Fig A.9a) under ambient conditions. Through its effect on root water uptake (Equation 7) ψ_c serves as an effective minimum soil water potential (outside of layers influenced by soil evaporation). In addition, due to the discontinuity of the root water uptake equation that occurs at ψ_c, soil water potential has a tendency to trend towards and then stick at ψ_c during dry periods. PHS instead adopts a more physical model for root water uptake (Equation 10) that avoids this discontinuity, preserves some soil moisture variability during dry periods (Figure 10), and better conforms to hydraulic theory.

5.5 The influence of soil moisture on transpiration

The stress effects of declining soil water potential seems to bias SMS predictions of transpiration relative to sap flux observations (Figure 14a,b). Under ambient conditions, soil water shows little relationship with sap flux observations with either model configuration (Supp Figure A.11b,f), however SMS modeled transpiration decreases strongly in response to soil drying (Supp Figure A.11a). This creates a bias where SMS underestimates transpiration during the drier soil conditions, which is in line with *Bonan et al.* [2014], where the water stress factor was found to impose too much attenuation of transpiration (in CLM4.5). With PHS the transpiration bias does not seem to strongly depend on soil potential, while also featuring less bias overall (Figure 14c,d). Likewise PHS yields a stronger relationship than SMS between soil potential and sap flux observations during TFE (Figure A.11d,h). This could indicate that PHS better models the relationship between soil potential and water stress and/or the soil moisture dynamics itself. The reduction in bias introduced by the water stress function (especially as it depends on soil potential) represents a major development, given repeated calls to improve vegetation water stress in the next generation of terrestrial biosphere models [*Powell et al.*, 2013; *Rogers et al.*, 2017].

5.6 Benefits and limitations of PHS

5.6.1 *Benefits*

1. Advances the physical basis of the CLM

   - Mechanistic xylem tension stress replaces empirical soil moisture stress

   - Root water uptake reflects established hydraulic theory

   - More appropriate response of water availability to root abundance

2. Improves modeled vegetation hydrodynamics

- Better match to observations of soil moisture and transpiration (higher correlation, lower RMSE)

- Importantly, the improvements modeling transpiration are achieved by removing a bias associated with soil water status

- Permits representation of compensatory root water uptake and hydraulic redistribution

- Avoids excessive soil layer drying observed with SMS

3. Creates an interface to new observational constraints

- Parameters are better represented in trait databases (e.g. k_{max}, p_{50}).

- New state variables modeling vegetation water potential are introduced, which are measured in situ and are shown to correlate with remote sensing products

- And given that vegetation water potential is downstream of soil water potential, this may actually provide an important constraint on root-zone soil moisture.

4. Enables a platform for testing various hydraulics-oriented hypotheses within the ESM context

- What are the relative contributions to water stress of VPD vs. soil moisture?

- Does the spectrum of isohydric vs. anisohydric regulation of vegetation water potential explain patterns in the terrestrial carbon and hydrological cycles?

- Are certain regions of the concatenated hydraulic-parameter / climate space particularly vulnerable to climate change?

5.6.2 Limitations

1. Plant hydraulics are highly simplified

- No capacitance

- Vulnerability not integrated across vegetation tissue or soil matrix

- Stem-to-leaf resistance is not fully deployed

- Simplified root system architecture

- These simplifications create a null hypothesis for further testing by the hydraulic community and yield a relatively light-weight model

2. Uncertainty regarding the parameterization of water stress

- PHS fits water stress (f_w) to leaf water potential via a sigmoidal function

- f_w is then used to attenuate V_{cmax}

- Many other approaches have been described in the literature, without a clear winner to date.

3. Increased model complexity

- Can potentially be mitigated by hydraulic trait coordination and improved priors and observational constraints on vegetation water potential

- Scale mismatch to reported parameter values in trait database

4. We don't provide a definitive assessment on model skill

- asymmetrical model tuning

- especially when taking into account the increased number of parameters

- however PHS offers better alignment with established theory and shows promising result in removing bias introduced by the water stress factor

6 Conclusion

The PHS configuration of the CLM5 within the Community Earth System Model (CESM)is, to our knowledge, the first land-surface model within an ESM with a representation of plant water potential running in its default configuration. In this paper, we have described the model implementation, and illustrated a comparison of the model dynamics for a tropical rainforest site subjected to water limitation, given that prediction of rainforest responses to drought is one of the key uncertainties in the ESM predictions [*Huntingford et al.*, 2013]. Overall, the new model behaviour differs from the default configuration in ways that are expected, given its structural properties, and in many cases, provides better correspondence with observations than the default structure.

In this paper, however, we did not aimed at undertaking a comprehensive assessment of which model structure performs better, given the substantial parametric uncertainty in both models, and the dependence on numerous other features of the CLM external to water stress representation that contribute to model-observation divergences - in this case in particular, the overestimation of unstressed transpiration by both versions of the model compared to the observations.

In lieu of this type of assessment, we propose that the new PHS model structure 1) is more closely aligned with known plant hydraulics theory, 2) provides significantly improved connections to real-world observational data streams (of leaf and stem water status, sap flow, percent loss conductance) and 3) represents known features of ecohydrological function that the default model cannot capture, including hydraulic redistribution, changes in the depth of water uptake with drought stress, plant embolism impacts on gas exchange and responses of water uptake to changes in leaf:root ratios.

7 Cut from other sections

In addition to modulating water stress and transpiration, vegetation water potential can be used to improve the CLM representation of root water uptake. PHS uses dynamic root water potential (ψ_{root}, Figure 6) as the sink for measuring the hydraulic gradient governing root water uptake ($\Delta\psi$). Because SMS does not resolve water potential through the vegetation substrate, the model instead uses a constant parameter, ψ_c, in its definition of $\Delta\psi$. As such, PHS provides a critical structural improvement for modeling root water uptake, consistent with extensive evidence of dynamic vegetation water potential (e.g. *Fisher et al.* [2006]).

Root water uptake dynamics are driven by either changes in $\Delta\psi$, as discussed above, or by changes in hydraulic conductance, k. PHS features mechanistic reductions in k based on root xylem vulnerability and soil hydraulic properties, conforming to soil-root hydraulic theory [*Cai et al.*, 2014; *Warren et al.*, 2015]. As a result the soil-root conductance features a strong, positive relationship with soil potential, decreasing by almost three orders of magnitude as the soil dries (Supp Fig A.6). Hydraulic conductance is not explicitly modeled with SMS, but the values implied by the transpiration partitioning function (see Section 2.4.2), actually increase as soils dry over the domain of $\psi_c < \psi_{\text{soil}} < \psi_o$ (Supp Fig A.6).

Furthermore, whereas SMS uses a relative notion to scale uptake by root abundance (root fraction), PHS opts for an absolute measure (root area), which can better capture dynamic carbon allocation in response to drying. With SMS, if root mass were to double in every soil layer, the root fraction remains unchanged, yielding no advantage in accessing soil water. With PHS, as root area in a soil layer increases so does the hydraulic conductance, even if the layer root fraction remains constant.

PHS appropriately penalizes extraction of soil water from deep in the soil column, associated with increased distance between roots, increased xylem length, and contributions from gravity (all factors not represented in SMS). As a result, PHS favors surface extraction when water is available (Figure A.3). The model can overcome these penalties, featuring

compensatory root water uptake where extraction (during the dry season) from beyond 2-meter depth increases significantly in response to TFE (Figure 12). Dynamic root water potential (and conductance) gives PHS more flexibility, allowing the model to switch root water uptake to the lower layers as the surface dries out.

Finally, PHS eschews the unsubstantiated constraints on $\Delta\psi$ imposed by SMS ($0 \geq \Delta\psi \geq \psi_c - \psi_o$, see Section 2.4.1). Allowing $\Delta\psi$ to change sign yields a representation of hydraulic redistribution, which has been observed in Amazonian forests [*Oliveira et al.*, 2005].

PHS uses leaf water potential (ψ_l) to calculate the water stress factor, replacing the previous version based on soil water potential (SMS). Using leaf water potential permits a representation of xylem tension stress and its diurnal variations, where vegetation must limit transpiration to avoid cavitation and embolism. This limitation is in addition to the VPD response of the Medlyn stomatal conductance model, which optimizes carbon gain versus water losses [*Medlyn et al.*, 2011]. Opting for xylem tension stress (PHS), in lieu of soil moisture stress (SMS), inserts an alternative physical interpretation of water stress and also yields different stress dynamics,

Basing stress on leaf water potential imparts a diurnal cycle to the water stress factor (Figure 7), following the midday drop in leaf water potential induced by high leaf-level VPD and photosynthesis. As such, water stress now depends on transpiration demand, and, in turn, leaf-level VPD and radiation (Figure 8, Supp Fig A.4) and not only on soil moisture stress. The PHS water stress factor also exhibits a seasonal cycle, with lower values (indicating more stress) during the dry season. However, the seasonal variation in water stress is smaller than with the control model (Figure 9a-d).

As a result, PHS (compared to SMS) features less seasonal variability in GPP and transpiration, especially under ambient conditions (Figures 9e-h, 3a,c). Furthermore, PHS exhibits less variability in transpiration than observations derived from sap flux velocity (Figure 3e,f). This follows from a negative feedback on GPP induced by the PHS water stress factor. Conditions favoring increased GPP (e.g. more light) also increase xylem tension and stress, which opposes increases in GPP. This negative feedback could be loosened by adjusting parameters to increase the hydraulic safety margin, such as increasing maximum stem hydraulic conductance. *Restrepo-Coupe et al.* [2017] show that GPP at Caxiuanã is highest during the dry season, suggesting that both models fail to capture the observed GPP seasonal cycle.

Likewise, both models produce a high bias in transpiration under TFE (Figure 3a,b). A previous study testing the CLM (version 3.5) with the Caxiuanã TFE experiment also found that the model underestimated the effect of the drought treatment [*Powell et al.*, 2013]. This might suggest model structural or parametrics deficiencies that are external to the water stress parameterization.

Overall, PHS provides a better match to sap flux observations, featuring lower RMSE and higher correlation, especially under ambient conditions. This result should be tempered by the fact that model tuning was not symmetrical between the two configurations (see Section 3). However, in Section 5.4, we discuss further evidence that suggests that PHS provides significant improvements in modeling water stress and its effect on transpiration.

The two models predict similar GPP during the TFE simulation (2002-2003), with 1.98 kgC/m^2/yr for SMS and 2.00 kgC/m^2/yr for PHS, but GPP is lower for PHS under ambient conditions (2.43 kgC/m^2/yr) as compared to SMS (2.73 kgC/m^2/yr, Figure 9e-h). Seasonal variability in GPP is smaller with PHS, especially under ambient conditions. The standard deviations of daily GPP (2002-2003) are 0.49 and 1.55 gC/m2/d for AMB/TFE, as compared to 1.53, 2.73 gC/m2/d with SMS. Lower maximal photosynthesis and less variability in GPP are both related to updates to the water stress factor implemented with PHS.

PHS has a stress response to high levels of transpiration (Supp Fig A.5c,d) due to the associated drops in leaf water potential. This negative feedback limits maximal transpiration and photosynthesis, while reducing variability. Transpiration shows a seasonal pattern in both models (Figure 3a,b), but with a larger amplitude for SMS. For example, under ambient conditions, the 10th and 90th percentiles for daily total transpiration with SMS are 1.65 and 4.22 mm/d (Δ=2.57 mm/d). That range exceeds the span for PHS: 1.85 and 3.49 mm/d (Δ=1.64 mm/d). Under ambient conditions, PHS underestimates transpiration variability as compared to sap flux observations (Figure 3e). However PHS yields a better overall fit to the field observations, with higher R^2 and lower RMSE compared to SMS under both ambient and TFE conditions (Figure 3c-f, Table 3).

Plant hydraulics can potentially improve model predictions of vegetation response to climate change [*Sperry and Love*, 2015], especially if parameter ranges and model complexity can be constrained [*Rogers et al.*, 2017]. Numerous site-level models have deployed plant hydraulics (e.g. *Williams et al.* [1996]; *Sperry et al.* [1998]; *Bohrer et al.* [2005]), and studies show vegetation water potential can improve predictions of stomatal response to the environment [*Sperry et al.*, 2017; *Anderegg et al.*, 2017], More recently hydraulics have been coupled to global models [*Bonan et al.*, 2014; *Xu et al.*, 2016; *Christoffersen et al.*, 2016], but most Earth System Models do not provide a mechanistic representation of vegetation water dynamics.

Incorporating hydraulic theory into Earth System Models is a well established ambition in the field of ecohydrology [*Sperry and Love*, 2015], supported by potential improvements in modeling mortality and productivity [*Choat et al.*, 2012; *McDowell et al.*, 2018]. However, concerns exist in the literature regarding hydraulic model complexity and parameterization [*Verhoef and Egea*, 2014; *Drake et al.*, 2017], which led to a series of simplifications implemented in our model design (see Section 2). Recent work suggests model complexity can be managed, given the significant coordination of hydraulic traits [*Bartlett et al.*, 2016; *Christoffersen et al.*, 2016]. Furthermore incorporating plant hydraulics provides access to new streams of observational data for model validation and parameterization. Vegetation water potential can be monitored in the field [*Boyer*, 1967] and has been shown to correlate with microwave remote sensing products [*Momen et al.*, 2017]. Parameter values can be measured in the field [*Sack et al.*, 2002] and are available in the TRY database [*Kattge et al.*, 2011].

Modeling stomatal conductance and photosynthesis, especially subject to water stress, is an area of ongoing research. We use the Medlyn VPD-dependence model coupled to a hydraulic stress function that attenuates V_{cmax}. This complies with observations [*Lin et al.*, 2018; *Zhou et al.*, 2013] that stress applied through g_1 underestimates attenuation of photosynthesis. However, there is no direct evidence of declines in V_{cmax} at the leaf level with drought [*Flexas et al.*, 2006], whereby future work may seek to represent mesophyll conductance in CLM to correct such discrepancy.

The model hydraulic supply representation is simplified, to reduce the model parameter and computational burdens. No capacitance. No integration of xylem or soil conductances vulnerability, instead based on lower node. No hysteresis in loss of conductance, xylem instantly regain conductance upon re-wetting. Leaf conductance simplified. Soil layers fully parallel, soil potential constant each time step.

Parameter uncertainty is significant. Notions of hydraulic architecture will never perfectly fit on this modeling scale, especially in a PFT paradigm. Field measurements of hydraulic traits will help constrain parameter ranges, but mostly only aboveground. Flux observations can help to tune stress parameters. Parameter estimation for root functioning is significantly more challenging, given the difficulty in underground trait observations. Likewise observational constraints of vertically-resolved states and fluxes underground are scarce. Follow-up work will be geared towards parameter estimation and assessing model skill.

902   Partitioned among the segments of the SPAC, the changes in leaf water potential (to-
903 taling -0.66MPa) due to TFE are: -0.44MPa soil potential, -0.66MPa soil-to-root, +0.45MPa
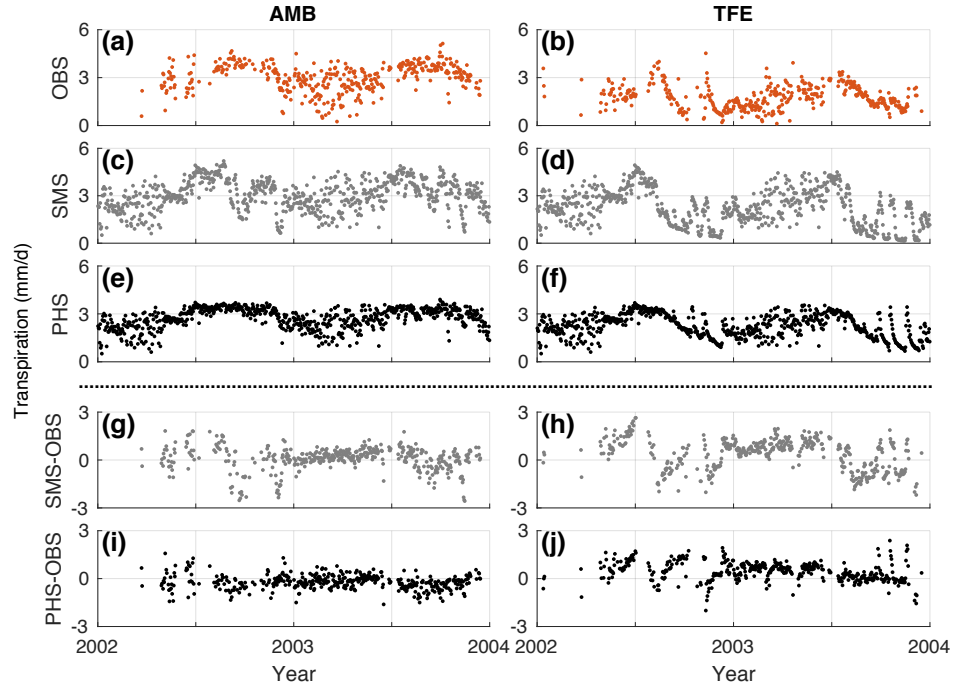904 root-to-stem, and -0.001MPa stem-to-leaf.

905 **8 Acknowledgments**

906 **9 Figures**
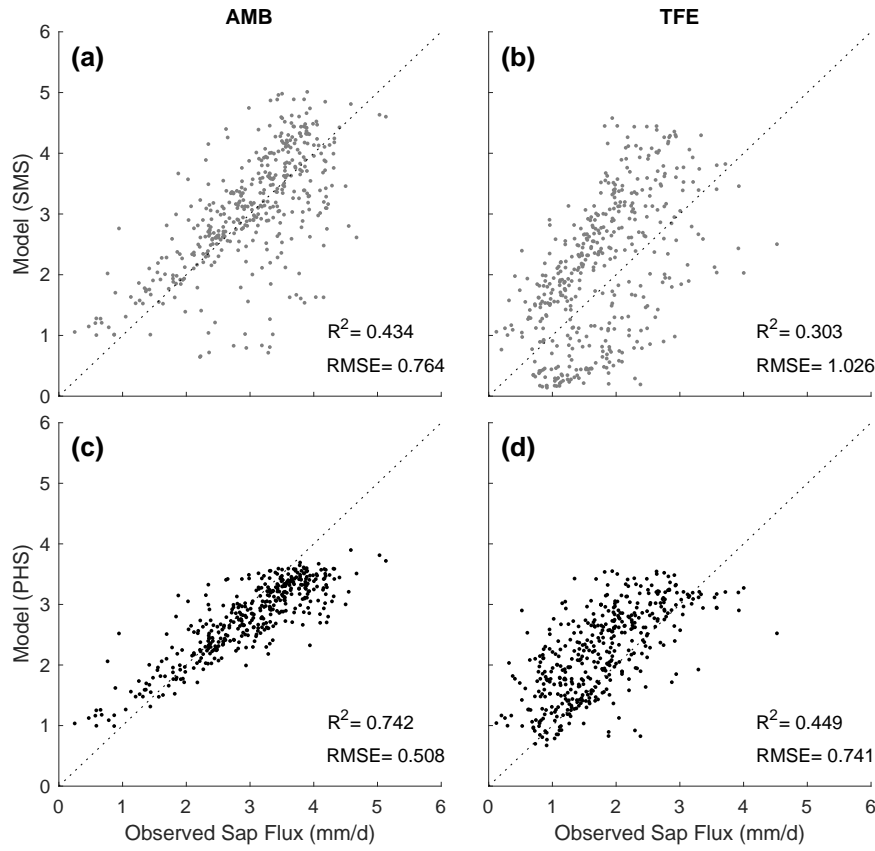
907 **Figure 3.** Modeled and observed daily total transpiration. Observations are derived from field observations
908 of sap flux velocity (see Section 3). (a,b) Modeled (lines, monthly mean) and observed (dots, daily total)
909 transpiration over time. (c-f) Modeled versus observed daily transpiration (mm/d).

Figure 4. Modeled and observed daily total transpiration. Observations are derived from field observations of sap flux velocity (see Section 3). (a,b) Modeled (lines, monthly mean) and observed (dots, daily total) transpiration over time. (c-f) Modeled versus observed daily transpiration (mm/d).
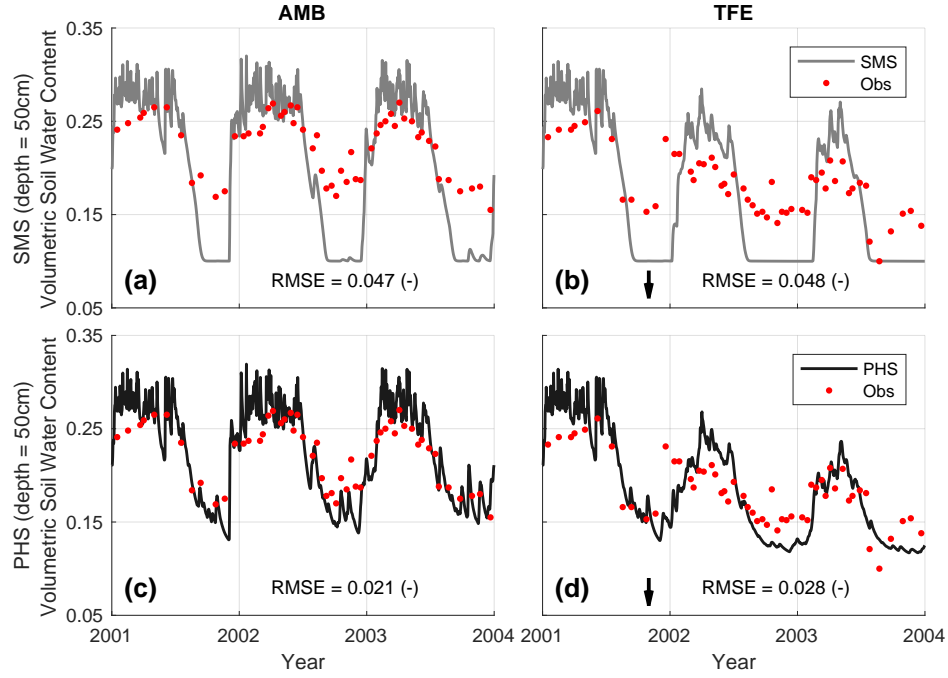
Figure 5. Volumetric soil water content (-) over time under ambient and TFE conditions at depth of 50cm. (a/b) SMS (c/d) PHS. RMSE are 0.048, 0.049, 0.022, and 0.029 [move to plot]. Arrows indicate start of TFE. Figure A.10 shows the same plots at 7 other soil depths.
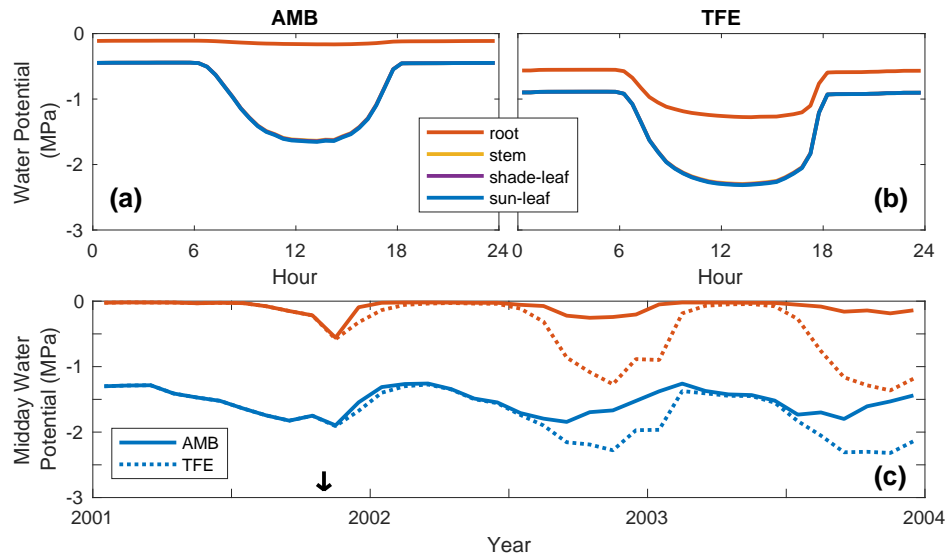
Figure 6. (a,b) 2003 dry season diurnal mean of modeled vegetation water potential under ambient and 60% TFE conditions. Curves are drawn for sunlit leaf, shaded leaf, stem, and root water potentials, with the latter three overlapping. (c) Monthly mean midday (12h-14h) vegetation water potential under ambient (solid line) and TFE (dotted line) conditions. Here curves are drawn only for sunlit leaf and root water potential. Note that TFE begins Nov 1, 2001, as indicated by the vertical arrow.
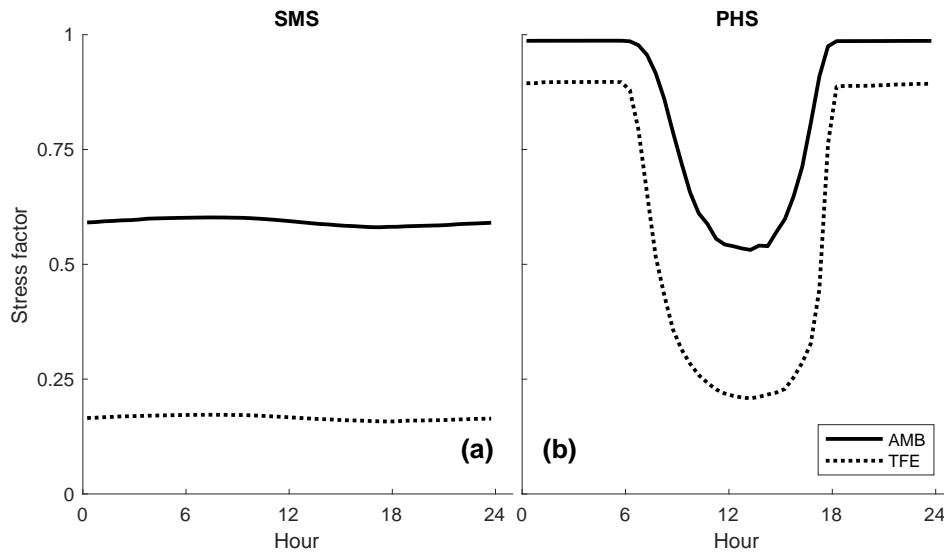
Figure 7. 2003 dry season (SON) diurnal mean water stress function for (a) SMS, and (b) PHS. Note that the water stress factor equals 1 when there is no stress and 0 when fully stressed.
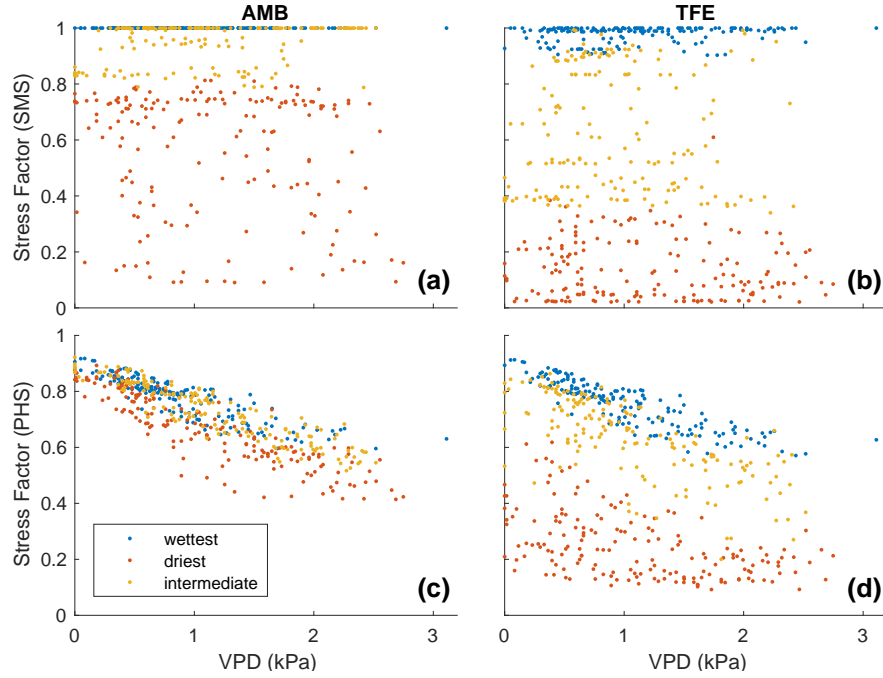
Figure 8. Water stress factor versus vapor pressure deficit (2002-2003), constrained to timesteps with downwelling shortwave radiation between 400 and 425 W/m2 (n=515). Radiation is controlled to highlight the relationship with VPD, the reverse (controlling for VPD) is shown in Figure A.4. For SMS (a,b), data are subdivided based on average soil matric potential, weighted by root fraction. For PHS (c,d), data are subdivided based on predawn (5h) root water potential. Blue dots represent the wettest tercile, yellow dots represent the intermediate tercile, and red dots represent the driest tercile (values defining each tercile are in Table 2).
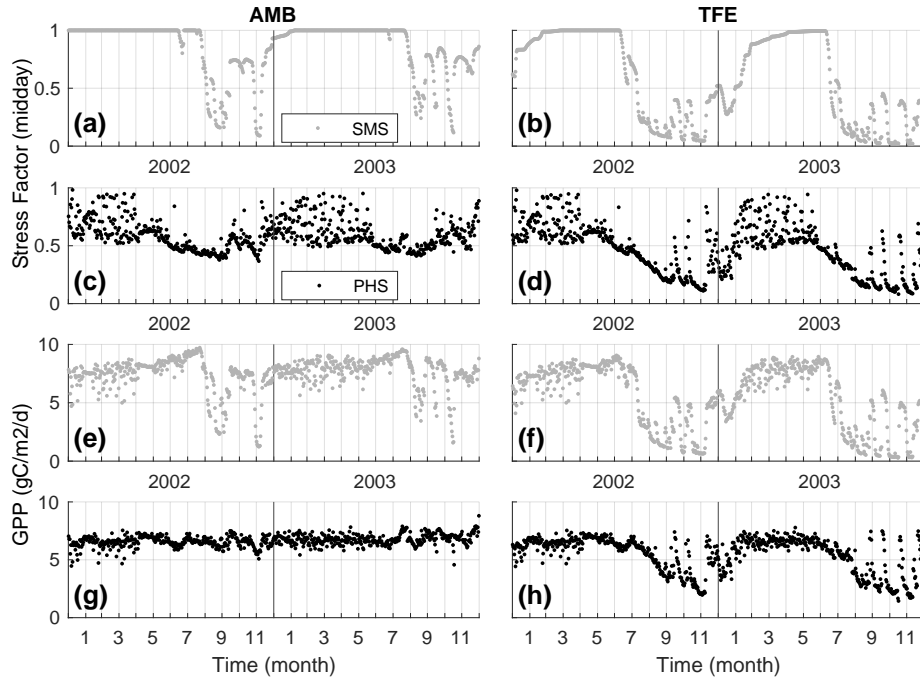
Figure 9. Daily stress factor (midday, averaged over 12h-14h) and GPP during 2002-2003 under ambient (left column) and TFE (right column) conditions. Output from the SMS configuration (a,b,e,f) are plotted with gray color, while output from the PHS configuration (c,d,g,h) are plotted in black.
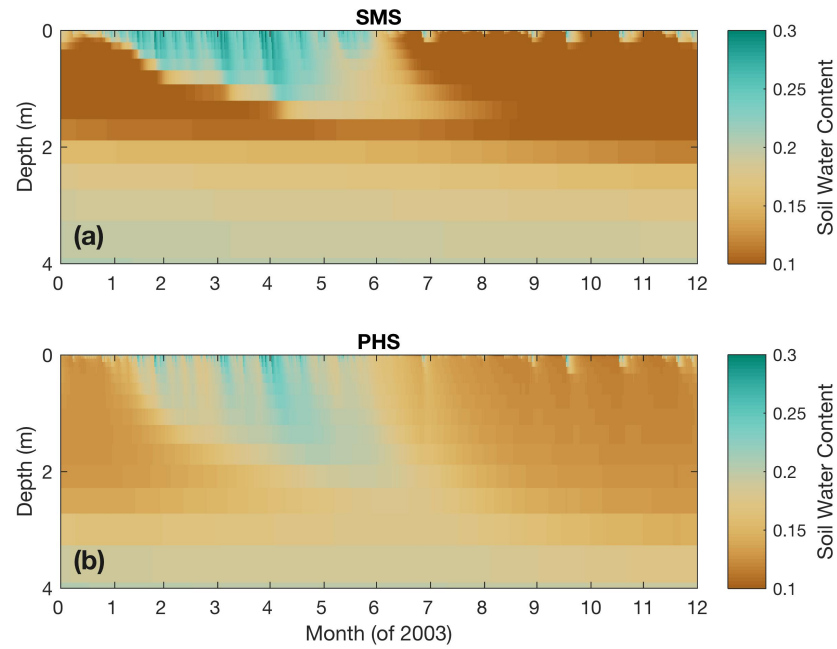
Figure 10. Vertical profile of soil water content (by volume) over time under 60% throughfall exclusion, for (a) SMS, and (b) PHS. Soil potential under ambient conditions is shown in Supp Fig A.9.
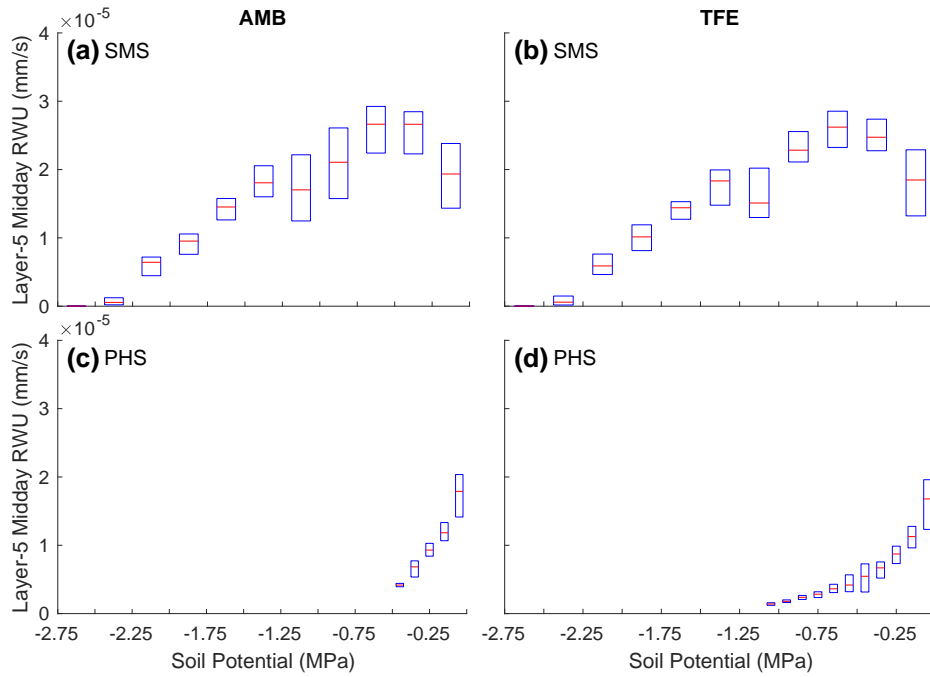
Figure 11. Binned boxplot of root water uptake versus soil potential for Soil Layer 5 (2002-3). Red lines mark the median, with boxes spanning the interquartile range. Bin widths are 0.25 MPa for SMS and 0.1 MPa for PHS. Soil Layer 5 is shown, because it is close enough to the surface (20 to 32 cm) to experience a significant range in soil potential, and it has a large root fraction (14.4%, only Soil Layer 6 has a larger root fraction). Only midday (12h-14h) timesteps are used to highlight the relationship with soil potential.
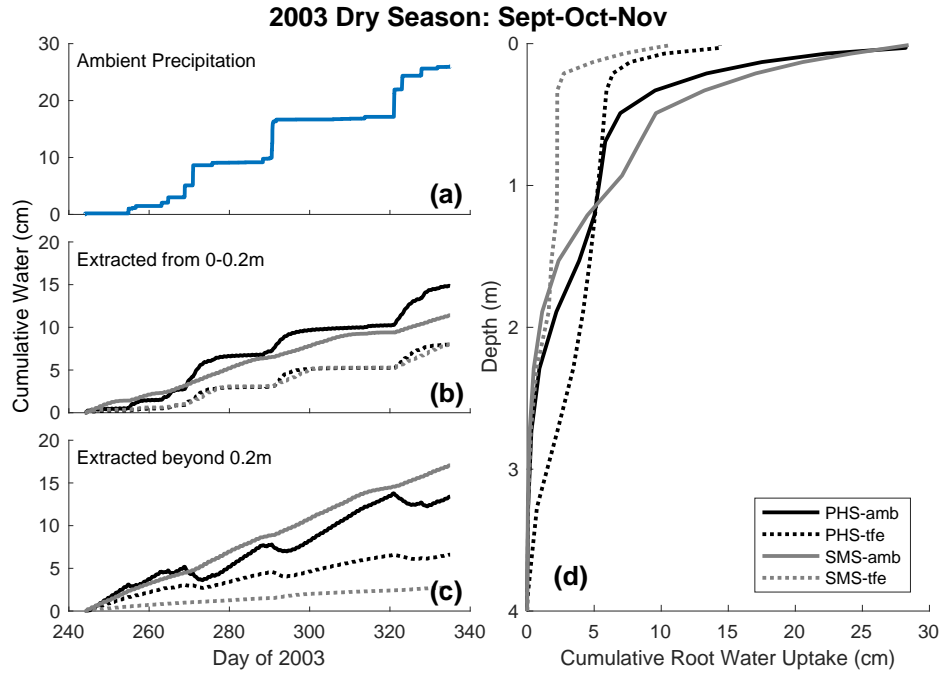
Figure 12. 2003 dry season (SON) cumulative root water uptake and precipitation. (a) Cumulative precipitation over time under ambient conditions (b,c) Cumulative water uptake over time from above and below 0.2m, respectively. (d) Cumulative root water uptake with depth.
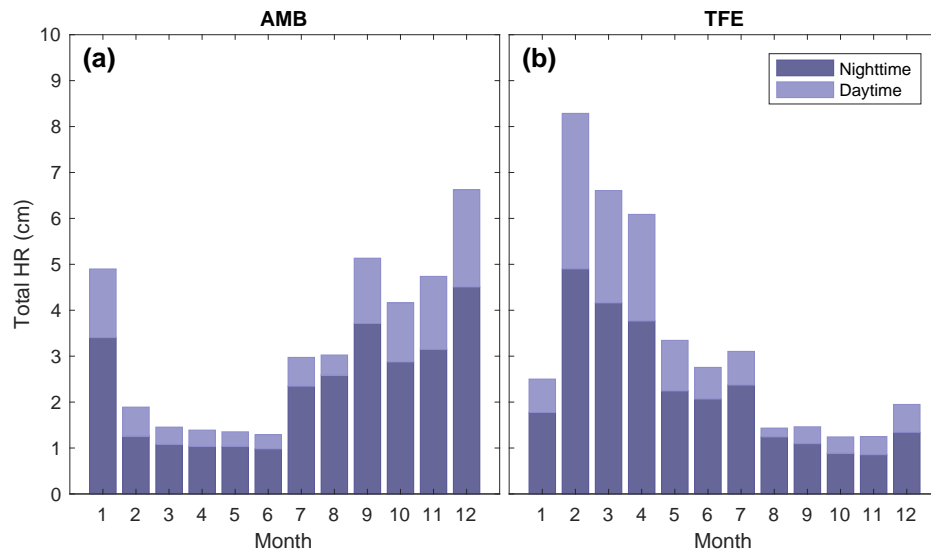
Figure 13. Total hydraulic redistribution (cm) by month across 2003. For (a) ambient through-fall conditions, and (b) 60% throughfall exclusion. Darker shading shows portion of HR at night [6pm,6am), lighter shading shows portion of HR during day [6am,6pm). Total HR refers to the sum of all negative root water uptake flows, when water is deposited by roots into a given soil layer.
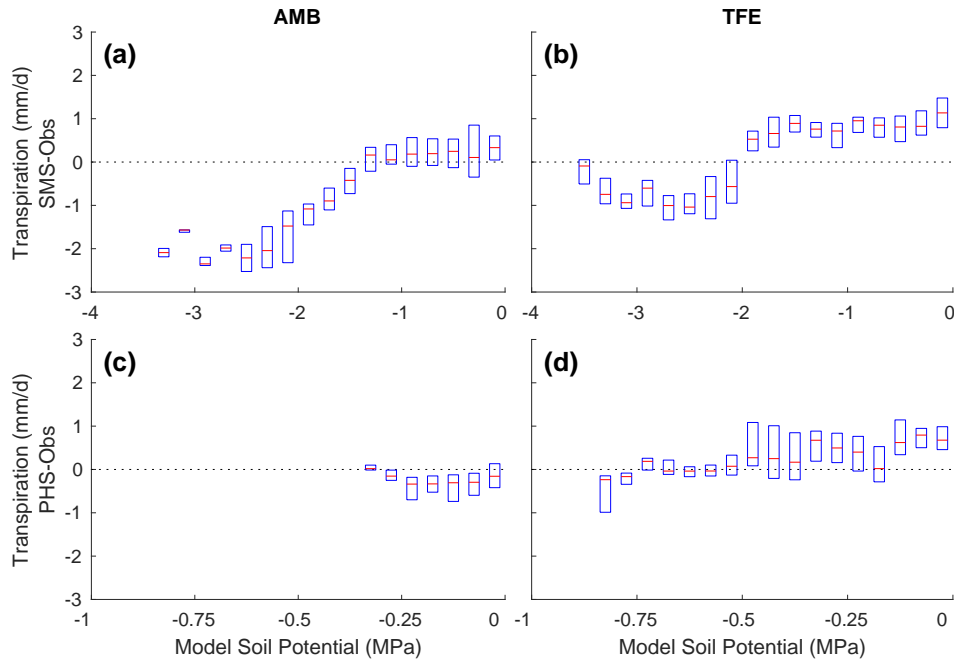
947 **Figure 14.** Binned boxplot showing the difference between modeled and observed transpiration (mm/d)
948 versus model soil potential. Red lines are drawn at the median, with boxes spanning the interquartile range.
949 The two models use different root water uptake paradigms, from which we define different operators for col-
950 umn effective soil potential. For SMS we average over the soil column weighted by root fraction and over time
951 (daily mean). For PHS we use predawn (5h) root water potential. Bin widths are 0.2 MPa for SMS (a,b) and
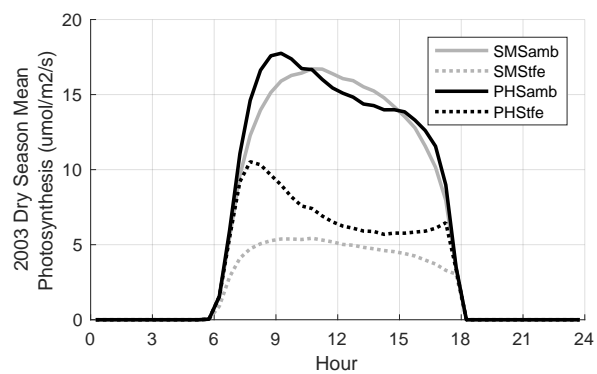952 0.05 MPa for PHS (c,d); note the different x-axes.
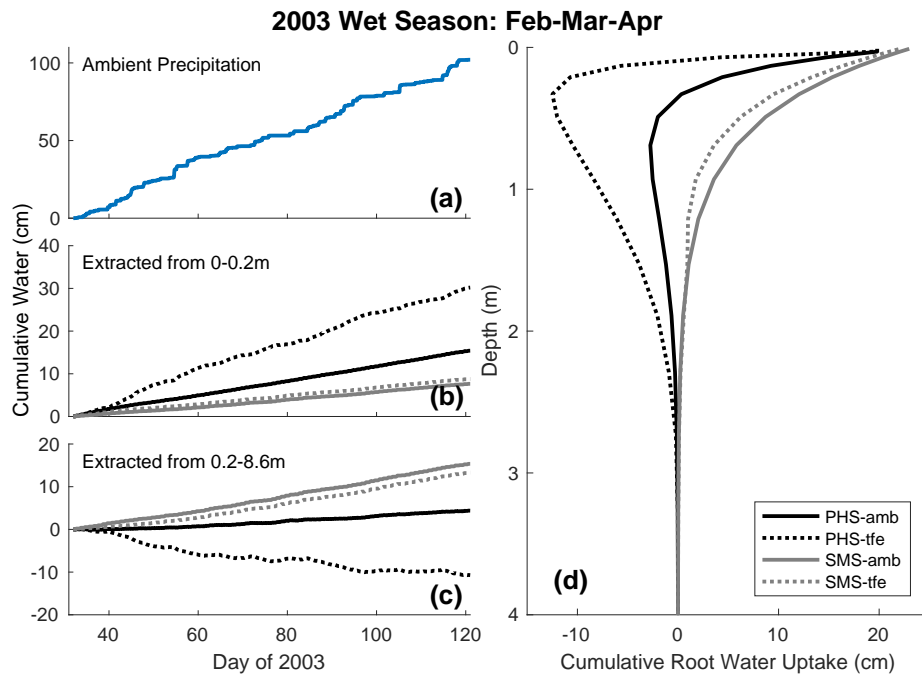
953 **A: Supplementary Figures**
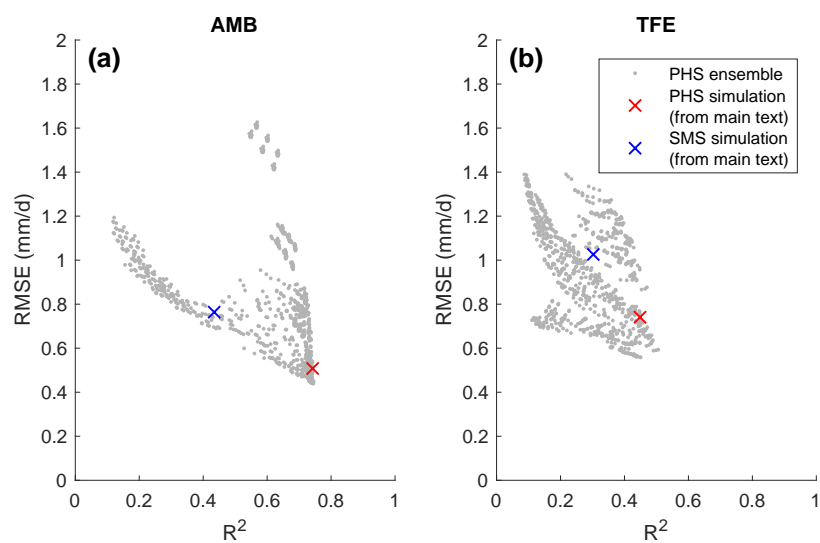

954 **Figure A.1.**   Parameter tuning exercise.

Figure A.2. 2003 dry season diurnal mean photosynthesis under ambient and TFE conditions for the two model configurations.

Figure A.3. 2003 wet season (FMA) cumulative root water uptake and precipitation. (a) Cumulative precipitation over time under ambient conditions (b,c) Cumulative water uptake over time from above and below 0.2m, respectively. (d) Cumulative root water uptake with depth.
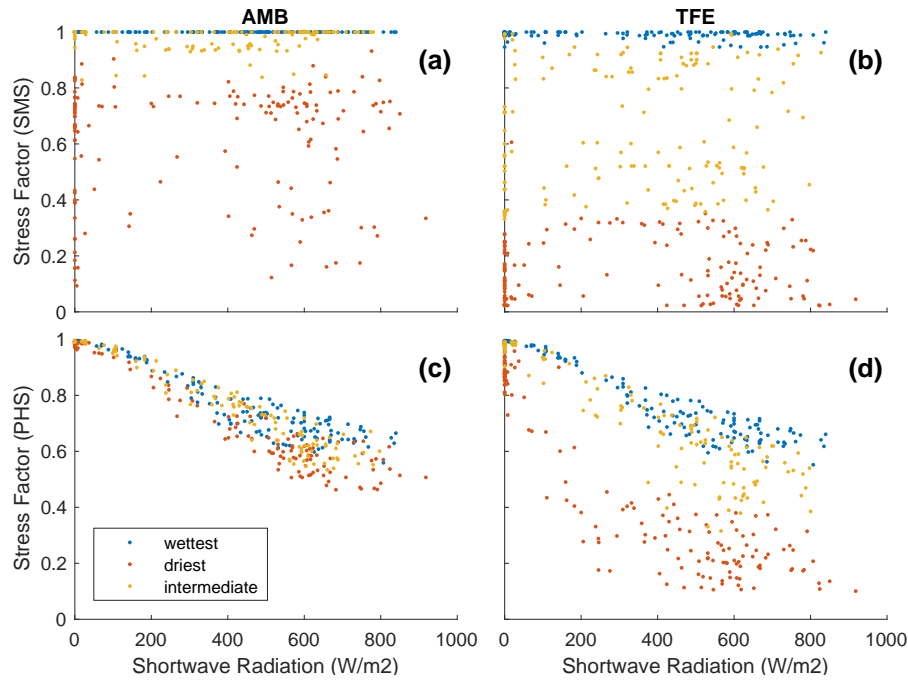
Figure A.4. Water stress factor versus downwelling shortwave radiation (2002-2003), for timesteps with VPD between 1 and 1.0559 kPa (n=470). VPD is controlled to highlight the relationship with downwelling radiation, the reverse (controlling for radiation) is shown in Figure 8. For SMS (a,b), data are subdivided based on average soil matric potential, weighted by root fraction. For PHS (c,d), data are subdivided based on predawn (5h) root water potential. Blue dots represent the wettest tercile, yellow dots represent the intermediate tercile, and red dots represent the driest tercile.
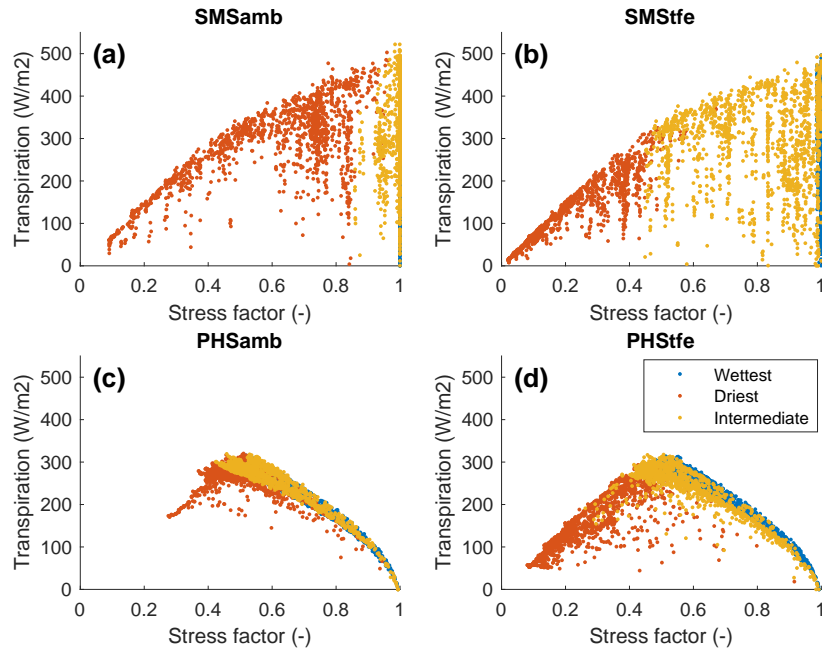
Figure A.5. Midday transpiration vs. stress. Data are colored by soil potential, subdivided into wettest, driest, and intermediate terciles.
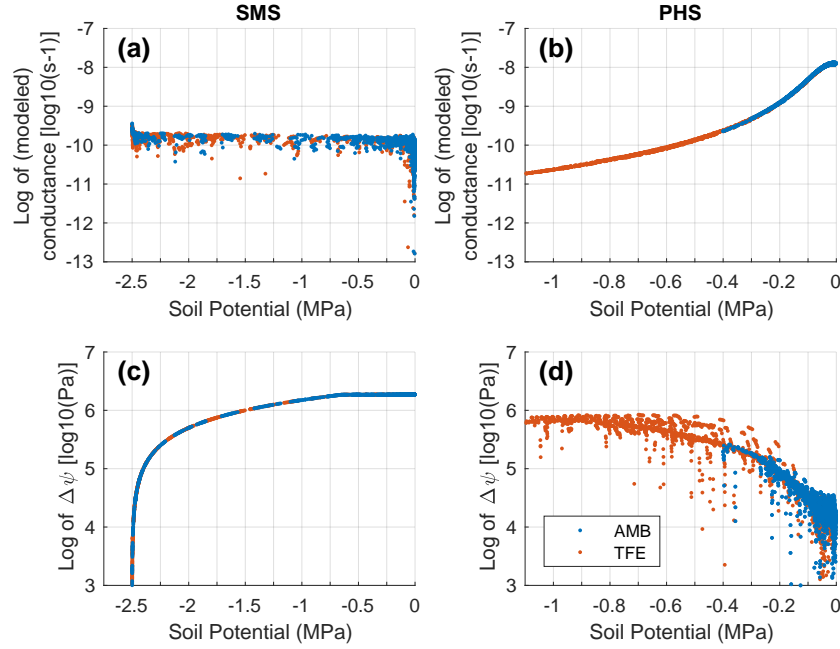
Figure A.6. (a,b) Log of conductance ($k_{s,r}$) versus soil potential for Soil Layer 5. (c,d) Log of hydraulic gradient ($\Delta\psi$) versus soil potential for Soil Layer 5. Note that the soil potential axes vary for PHS vs. SMS. Multiplied together $k_{s,r}$ and $\Delta\psi$ yield the Layer-5 root water uptake. PHS conductance decreases by almost 3 orders of magnitude between 0 and -1MPa, which leads to reduced RWU, though this is offset (by about half) due to increases in $\Delta\psi$.

while SMS $\Delta\psi$ decreases by less than 1 order of magnitude between 0 and -2MPa, leading to higher sensitivity to soil potential with PHS, see Figure 11.

Only midday (12h-14h, 2002-2003) timesteps are shown to emphasize the relationship with soil potential. With SMS, conductance is not modeled explicitly, but rather calculated as $k=q/\Delta\psi$ (see Section zqz). For soil potentials greater than or equal to 2.5MPa, $\Delta\psi$=0, and SMS implied conductance is undefined, but could probably be considered to equal 0. PHS conductance captures both root tissue and soil matrix resistances (operating in series).
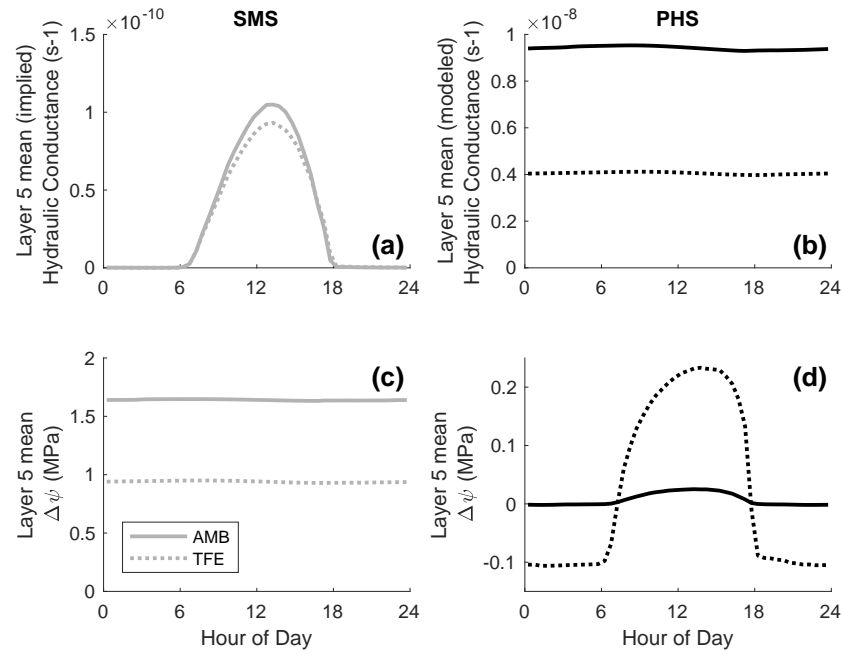
Figure A.7. 2003 diurnal mean of Soil Layer 5 conductance and $\Delta\psi$, under ambient and TFE conditions.
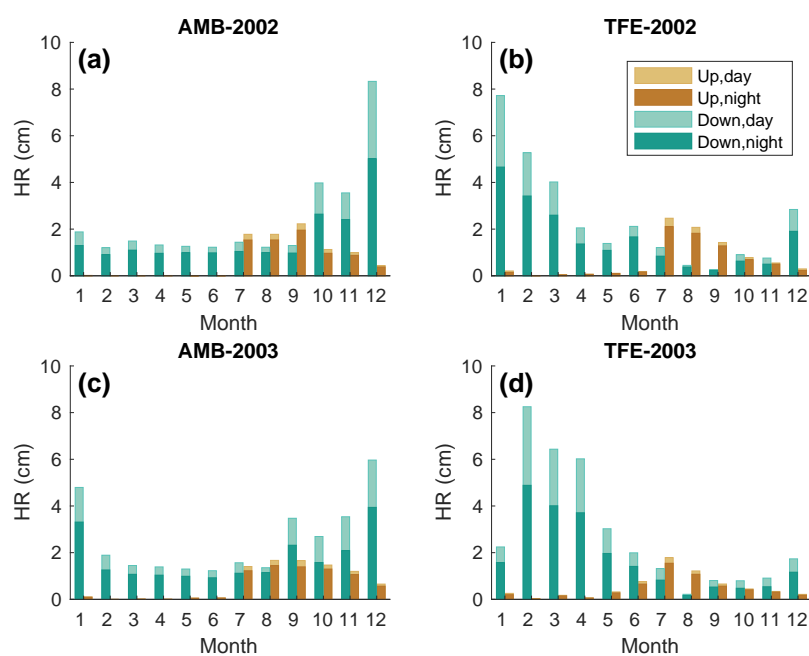
Figure A.8. PHS hydraulic distribution during 2003. Alternative version partitioning by direction.
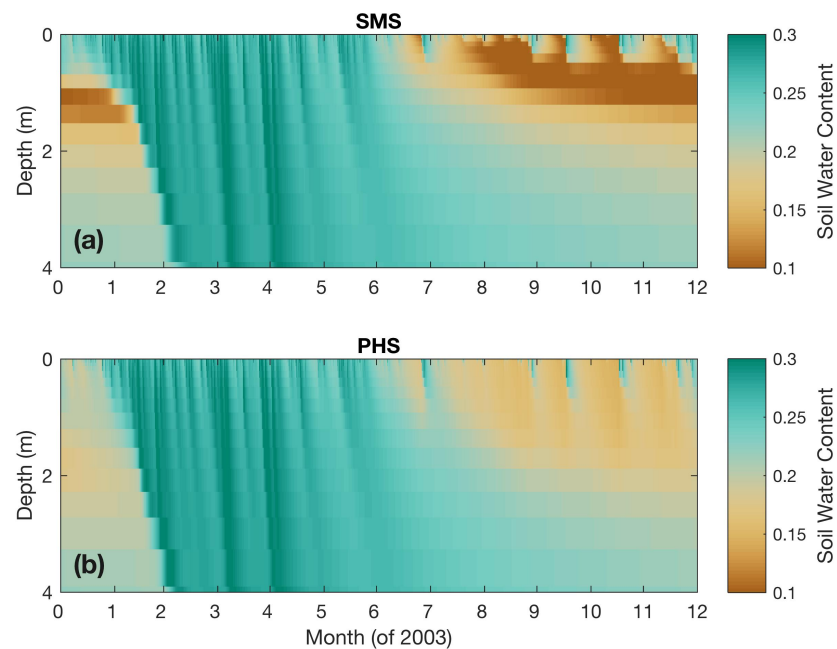
Figure A.9. Vertical profile of soil water content (by volume) through time under ambient through-fall conditions, for (a) PHS, and (b) SMS.
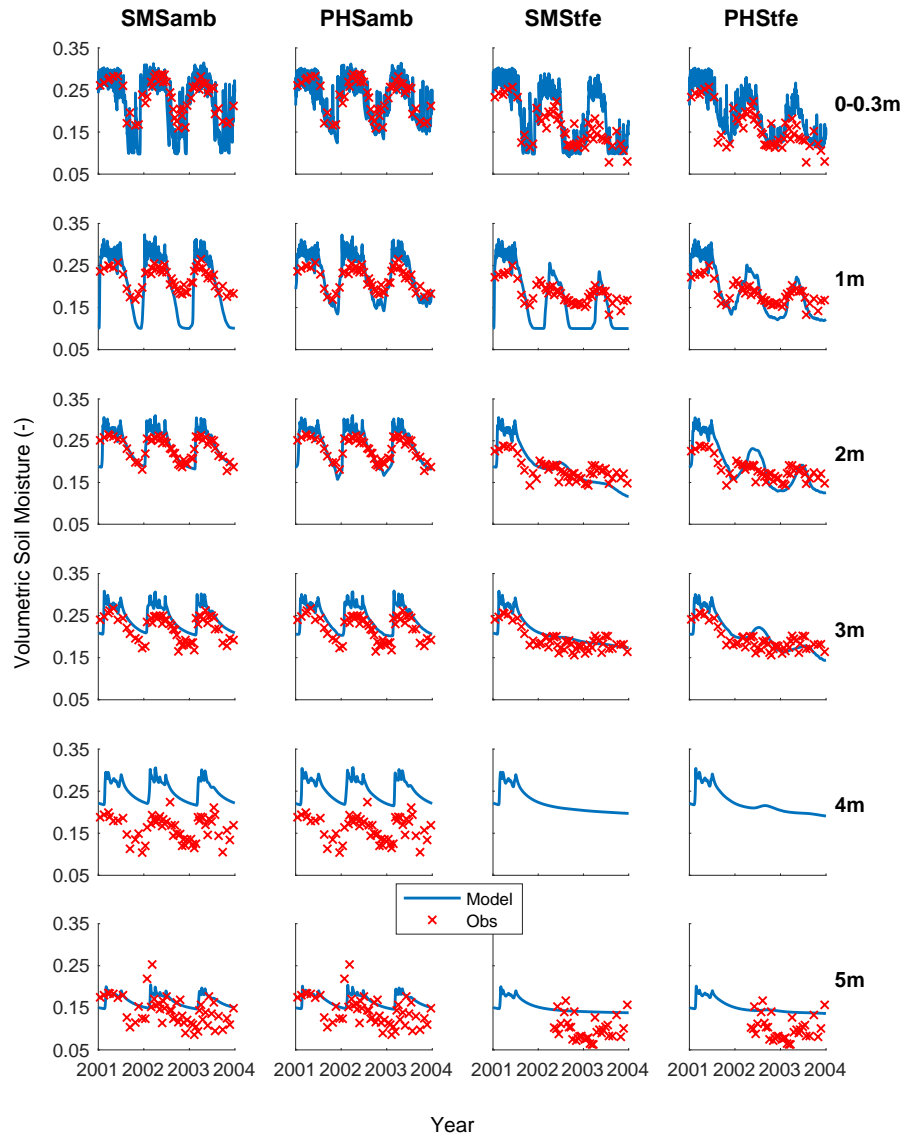
Figure A.10. Time series of soil moisture by soil layer. Complements Figure 10

Figure A.11. Modeled (left column) and observed (right column) transpiration vs. model soil potential. Complements Figure 14

B: Appendix to Model Description

B.1 Details of Water Supply

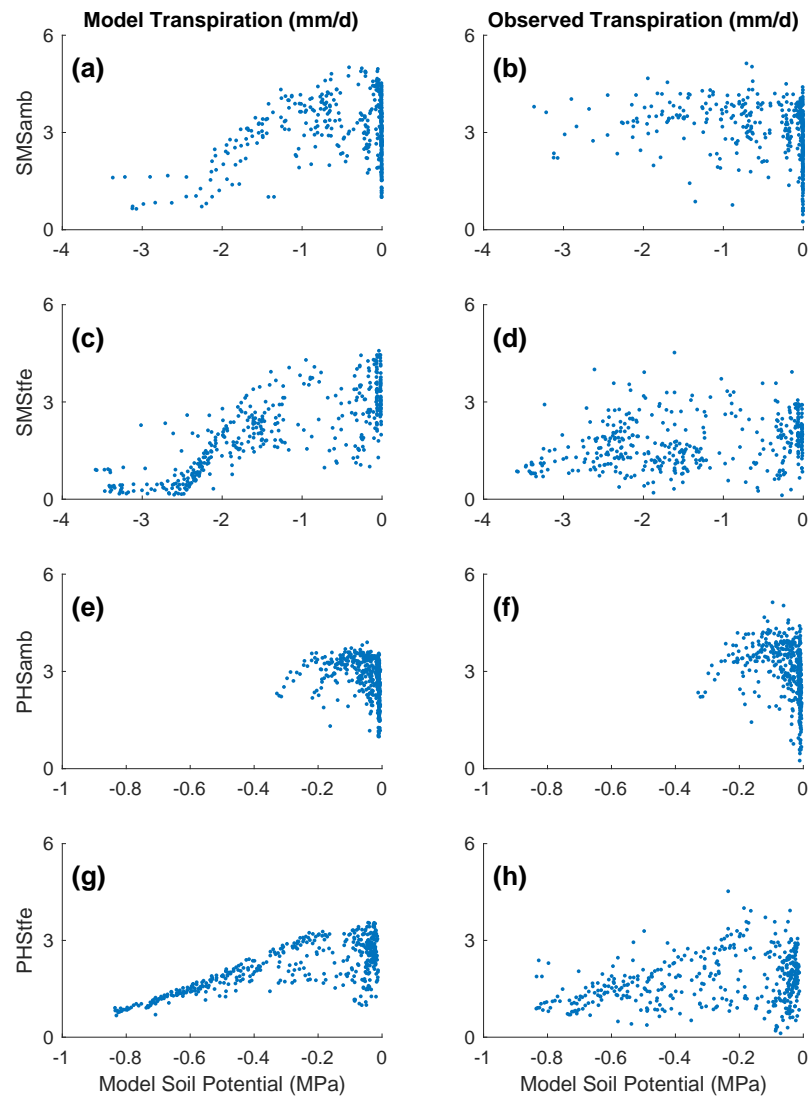PHS resolves flow across four different segments, soil-to-root, root-to-stem, stem-to-leaf, and leaf-to-transpiration.

Stem-to-leaf. The area bases are sunlit and shaded leaf area, respectively. Note that gravity is assumed negligible here. Likewise there is no length scaling applied to maximum conductance. Therefore the input parameter for $k_{leaf,\max}$ should be a conductance (s^{-1}).

$$q_{sun} = k_{sun} \cdot \text{LAI-sun} \cdot (\psi_{\text{stem}} - \psi_{\text{sun-leaf}})$$
$$q_{shade} = k_{shade} \cdot \text{LAI-shade} \cdot (\psi_{\text{stem}} - \psi_{\text{shade-leaf}}) \tag{B.1}$$

$$k_{sun} = k_{shade} = k_{leaf,\max} \cdot f(\psi_{\text{stem}}) \tag{B.2}$$

$$f(\psi) = 2^{-\left(\frac{\psi}{p_{50}}\right)^{c_k}} \tag{B.3}$$

Root-to-stem. The area basis is stem area index. The input parameter is maximum stem xylem conductivity ($K_{stem,\max}$). Stem conductance (k_{stem}) is the result of scaling maximum conductivity by the tree height (h) and applying loss relative to maximum conductance via the vulnerability curve $f(\psi_{\text{root}})$.

$$q_{stem} = k_{stem} \cdot \text{SAI} \cdot (\psi_{\text{root}} - \psi_{\text{stem}} - \rho g h) \tag{B.4}$$

$$k_{stem} = \frac{K_{stem,\max}}{h} \cdot f(\psi_{\text{root}}) \tag{B.5}$$

Soil-to-root. Area basis is RAI in soil layer i, which is based on the layer root fraction times the total root area. Total root area is calculated as the sum of stem and leaf area indices multiplied by a relative root area parameter (f_{root}). The vertical root distribution is defined by the layer root fraction (r_i), which follows a one-parameter (by PFT) power law decay following *Jackson et al.* [1996].

$$q_{sr,i} = k_{sr,i} \cdot \text{RAI}_i \cdot (\psi_{\text{soil,i}} - \psi_{\text{root}} - \rho g z_i) \tag{B.6}$$

$$\text{RAI}_i = f_{\text{root}} \cdot (\text{SAI} + \text{LAI}) \cdot r_i \tag{B.7}$$

$$k_{sr,i} = \frac{k_{r,i} + k_{s,i}}{k_{r,i} \cdot k_{s,i}} \tag{B.8}$$

$$k_{r,i} = \frac{K_{r,\max}}{l_i} f(\psi_{\text{soil,i}}) \tag{B.9}$$

$$l_i = z_i + x \tag{B.10}$$

$$k_{s,i} = \frac{K_{s,i}}{d} \tag{B.11}$$

The soil-and-root conductance $k_{sr,i}$ reflects two resistors in series, from soil-to-root ($k_{s,i}$) and through the root tissue ($k_{r,i}$). The root tissue conductance is attenuated via the vulnerability curve framework. The input parameter is maximum root xylem conductivity, on the basis of RAI as defined above. The root conductivity is scaled by the conducting length, which is estimated as the sum of soil layer depth (z_i) and average lateral extent (x, static parameter). The soil conductivity $K_{s,i}$ is calculated from the layer soil matric potential ($\psi_{soil,i}$) and soil properties as described in *Oleson et al.* [2013] utilizing typical soil hydraulic theory [*Brooks and Corey*, 1964; *Clapp and Hornberger*, 1978]. The soil conductance ($k_{s,i}$) is the result of scaling the conductivity by d, the distance between roots estimated following *Williams et al.* [1996] and *Bonan et al.* [2014]

B.2 Details of Water Demand

The CLM5 implementation utilizes the Medlyn stomatal conductance model [*Medlyn et al.*, 2011], while also applying water stress through V_{cmax}. Transpiration is calculated reflecting contributions from both stomatal conductance and leaf boundary layer conductance (g_b).

$$V_{cmax} = f_w V_{cmax,ww} \qquad (B.12)$$

$$g_s = g_0 + \left(1 + \frac{g_1}{\sqrt{D}}\right) \frac{A}{C_a} \qquad (B.13)$$

$$E_{sun} = g_{s,sun} * \rho * \text{VPD} * lai_{sun} * \left(1 + \frac{g_{s,sun}}{g_b}\right)^{-1}$$
$$E_{shade} = g_{s,shade} * \rho * \text{VPD} * lai_{shade} * \left(1 + \frac{g_{s,shade}}{g_b}\right)^{-1} \qquad (B.14)$$

At the beginning of a set of PHS iterations, we solve for $E_{sun,max}$ and $E_{shade,max}$, by running the stomatal conductance scheme with f_w set to 1 (no stress). Within each PHS iteration, we do not resolve the full stomatal conductance scheme, but instead consider only the linear attenuation of stomatal conductance by f_w. Transpiration is attenuated relative to the maximal values according to leaf water potential.

$$E_{sun} = E_{sun,max} * 2^{-\left(\frac{\psi_{leaf}}{\psi_{50}}\right)^{c_k}}$$
$$E_{shade} = E_{shade,max} * 2^{-\left(\frac{\psi_{leaf}}{\psi_{50}}\right)^{c_k}} \qquad (B.15)$$

We define f_w as the ratio of attenuated stomatal conductance ($g_{s,sun}$, $g_{s,shade}$) to maximal stomatal conductance ($g_{s,sun,max}$, $g_{s,shade,max}$), where $g_{s,sun,max}$ and $g_{s,shade,max}$ are the stomatal conductance values associated with $E_{sun,max}$ and $E_{shade,max}$. As such, the definition in the main text (Equation 13), represents a linear simplification between f_w, stomatal conductance, and transpiration.

$$f_{w,sun} = \frac{g_{s,sun}}{g_{s,sun,max}}$$
$$f_{w,shade} = \frac{g_{s,shade}}{g_{s,shade,max}} \qquad (B.16)$$

After each PHS iteration, we compute $g_{s,sun}$ and $g_{s,shade}$ via Equations B.12 and B.12 (which involves iterating for intercellular CO_2 concentration). We then update $g_{s,sun,max}$ and $g_{s,shade,max}$ to achieve consistency between equations (B.14) and (B.15). At this point $g_{s,sun,max}$ and $g_{s,shade,max}$ no longer refer to the values associated with $f_w = 1$, but rather also incorporate the non-linearity between g_s and f_w. The PHS iteration continues to convergence of f_w (see Figure B.1). The numerics have proven to be stable in practice, but future versions may aim to better integrate PHS within the stomatal conductance scheme to improve the coherence of Equations 13 and B.16.

$$g_{s,sun,max} = \frac{g_{s,sun}}{f_{w,sun}}$$
$$g_{s,shade,max} = \frac{g_{s,shade}}{f_{w,shade}} \qquad (B.17)$$

Calculate metabolic parameters $(V_{cmax}, J_{max}, R_d, K_c, K_o, \Gamma_*)$ ← Initial T_l

Initial C_i

Set $f_{w,sun}$ and $f_{w,shade}$ = 1

Calculate assimilation $(A_{n,max})$, stomatal conductance $(g_{s,sun,max}, g_{s,shade,max})$, transpiration $(T_{sun,max}, T_{shade,max})$ [absent water stress]

Calculate C_i

c_i convergence? — no

Initial C_i

PHS solves for ψ and f_w

Calculate assimilation (A_n) and stomatal conductance $(g_{s,sun}, g_{s,shade})$ using f_w [includes water stress]

Calculate C_i

c_i convergence? — no

f_w convergence? — no — Update $g_{s,sun,max}$ & $g_{s,shade,max}$

Calculate leaf temperature (T_l) and fluxes $(H_l, \lambda E_l)$

no — T_l convergence?

Figure B.1. Flow chart of PHS iterative solution

1053

B.3 Details of Water Potential Solution

The continuity of water flow through the system yields four equations

$$E_{sun} = q_{sun}$$
$$E_{shade} = q_{shade}$$
$$q_{sun} + q_{shade} = q_{stem} \tag{B.18}$$
$$q_{stem} = \sum_{i=1}^{nlevsoi} q_{sr,i}$$

We seek the set of vegetation water potential values (four unknowns),

$$\psi = \begin{bmatrix} \psi_{sunleaf} \\ \psi_{shadeleaf} \\ \psi_{stem} \\ \psi_{root} \end{bmatrix} \tag{B.19}$$

that satisfies these equations, as forced by the soil moisture and atmospheric state.

Each flux on the schematic can be represented in terms of the relevant water potentials.

Defining the transpiration fluxes:

$$E_{sun} = E_{sun,max} \cdot 2^{-\left(\frac{\psi_{sunleaf}}{p50}\right)^{c_k}} \tag{B.20}$$
$$E_{shade} = E_{shade,max} \cdot 2^{-\left(\frac{\psi_{shadeleaf}}{p50}\right)^{c_k}}$$

Defining the water supply fluxes:

$$q_{sun} = k_{leaf,max} \cdot 2^{-\left(\frac{\psi_{stem}}{p50}\right)^{c_k}} \cdot \text{LAI}_{sun} \cdot \left(\psi_{stem} - \psi_{sunleaf}\right)$$
$$q_{shade} = k_{leaf,max} \cdot 2^{-\left(\frac{\psi_{stem}}{p50}\right)^{c_k}} \cdot \text{LAI}_{shade} \cdot \left(\psi_{stem} - \psi_{shadeleaf}\right)$$
$$q_{stem} = \frac{k_{stem,max}}{z_2} \cdot 2^{-\left(\frac{\psi_{root}}{p50}\right)^{c_k}} \cdot SAI \cdot \left(\psi_{root} - \psi_{stem} - \Delta\psi_z\right) \tag{B.21}$$
$$q_{root} = \sum_{i=1}^{nlevsoi} q_{sr,i} = \sum_{i=1}^{nlevsoi} k_{sr,i} \cdot RAI \cdot \left(\psi_{soil,i} - \psi_{root} + \Delta\psi_{z,i}\right)$$

In the CLM parameter file, $p50$ and c_k are allowed to vary by flux level (transpiration vs. stem flux vs. root flux), but in our experiment (and on the default CLM parameter file), a single value is used for each. PHS solves for the vector ψ that satisfying water flow continuity as forced by atmospheric state and soil moisture. Due to the model non-linearity, we use a linearized explicit approach, iterating with Newton's method. The initial guess is the solution for ψ (vector) from the previous time step. The general framework, from iteration m to $m + 1$ is:

$$q^{m+1} = q^m + \frac{\delta q}{\delta \psi}\Delta\psi \tag{B.22}$$
$$\psi^{m+1} = \psi^m + \Delta\psi$$

So for our first flux balance equation, which requires sunlit leaf transpiration equal the flux of water from the main stem to the sunlit leaf, we have (at iteration $m + 1$):

$$E_{sun}^{m+1} = q_{sun}^{m+1} \tag{B.23}$$

This can be linearized to:

$$E_{sun}^m + \frac{\delta E_{sun}}{\delta \psi} \Delta \psi = q_{sun}^m + \frac{\delta q_{sun}}{\delta \psi} \Delta \psi \tag{B.24}$$

And rearranged to be:

$$\frac{\delta q_{sun}}{\delta \psi} \Delta \psi - \frac{\delta E_{sun}}{\delta \psi} \Delta \psi = E_{sun}^m - q_{sun}^m \tag{B.25}$$

And for the other 3 flux balance equations:

$$\frac{\delta q_{shade}}{\delta \psi} \Delta \psi - \frac{\delta E_{sha}}{\delta \psi} \Delta \psi = E_{sha}^m - q_{1b}^m$$
$$\frac{\delta q_{stem}}{\delta \psi} \Delta \psi - \frac{\delta q_{sun}}{\delta \psi} \Delta \psi - \frac{\delta q_{shade}}{\delta \psi} \Delta \psi = q_{sun}^m + q_{shade}^m - q_{stem}^m \tag{B.26}$$
$$\frac{\delta q_{soil}}{\delta \psi} \Delta \psi - \frac{\delta q_{stem}}{\delta \psi} \Delta \psi = q_{stem}^m - q_{soil}^m$$

Putting all four together in matrix form:

$$\begin{bmatrix} \frac{\delta q_{1a}}{\delta \psi} - \frac{\delta E_{sun}}{\delta \psi} \\ \frac{\delta q_{1b}}{\delta \psi} - \frac{\delta E_{sha}}{\delta \psi} \\ \frac{\delta q_2}{\delta \psi} - \frac{\delta q_{1a}}{\delta \psi} - \frac{\delta q_{1b}}{\delta \psi} \\ \frac{\delta q_{soil}}{\delta \psi} - \frac{\delta q_2}{\delta \psi} \end{bmatrix} \Delta \psi = \begin{bmatrix} E_{sun}^m - q_{1a}^m \\ E_{sha}^m - q_{1b}^m \\ q_{1a}^m + q_{1b}^m - q_2^m \\ q_2^m - q_{soil}^m \end{bmatrix} \tag{B.27}$$

Now to expand the left-hand side, from vector ψ to the four distinct plant water potential nodes, noting that many derivatives are zero (e.g. $\frac{\delta E_{sun}}{\delta \psi_{sha}} = 0$)

Introducing the notation: $A \Delta \psi = b$

$$\Delta \psi = \begin{bmatrix} \Delta \psi_{sunleaf} \\ \Delta \psi_{shadeleaf} \\ \Delta \psi_{stem} \\ \Delta \psi_{root} \end{bmatrix} \tag{B.28}$$

$$A = \begin{bmatrix} \frac{\delta q_{1a}}{\delta \psi_{sun}} - \frac{\delta E_{sun}}{\delta \psi_{sun}} & 0 & \frac{\delta q_{1a}}{\delta \psi_{stem}} & 0 \\ 0 & \frac{\delta q_{1b}}{\delta \psi_{sha}} - \frac{\delta E_{sha}}{\delta \psi_{sha}} & \frac{\delta q_{1b}}{\delta \psi_{stem}} & 0 \\ -\frac{\delta q_{1a}}{\delta \psi_{sun}} & -\frac{\delta q_{1b}}{\delta \psi_{sha}} & \frac{\delta q_2}{\delta \psi_{stem}} - \frac{\delta q_{1a}}{\delta \psi_{stem}} - \frac{\delta q_{1b}}{\delta \psi_{stem}} & \frac{\delta q_2}{\delta \psi_{root}} \\ 0 & 0 & -\frac{\delta q_2}{\delta \psi_{stem}} & \frac{\delta q_{soil}}{\delta \psi_{root}} - \frac{\delta q_2}{\delta \psi_{root}} \end{bmatrix} \tag{B.29}$$

$$b = \begin{bmatrix} E_{sun}^m - q_{b1}^m \\ E_{sha}^m - q_{b2}^m \\ q_{b1}^m + q_{b2}^m - q_{stem}^m \\ q_{stem}^m - q_{soil}^m \end{bmatrix} \quad (B.30)$$

We can compute all the entries for A and b based on the soil potential and maximum transpiration forcings and can solve to find:

$$\Delta\psi = A^{-1}b \quad (B.31)$$

$$\psi_{m+1} = \psi_m + \Delta\psi \quad (B.32)$$

We iterate until $b \to 0$, signifying water flux balance through the system. The result is a final set of water potentials ($\psi_{root}, \psi_{stem}, \psi_{shadeleaf}, \psi_{sunleaf}$) satisfying non-divergent water flux through the system.

B.4 Parameter tuning exercise

We used a factorial design to create 972 ensemble members based on the parameter values below. We ran PHS simulations for each parameter vector under both AMB and TFE conditions. All simulations used the same initial conditions, which were the result of a previous simulation. We evaluated the ensemble members based on the fit to sap flux observations, selecting that which maximized $R^2_{amb} + R^2_{tfe} - RMSE_{amb} - RMSE_{tfe}$ (Supp Fig A.1).

Stem conductivity, k_{max}: 2e-8, 4e-8, 8e-8 s^{-1}
Root conductivity, $k_{r,max}$: 2e-9, 6e-8, 18e-9 s^{-1}
Root and stem vulnerability p_{50}: -1.75, -2.25, -2.75 MPa
Stomatal p_{50}: above plus either 0 or 0.5MPa
Vulnerability shape parameter, c_k: 2.95, 3.95, 5.45 (unitless)
Medlyn slope, g_1: 6, 7 kPa$^{0.5}$
Rooting depth parameter, β: 0.95, 0.98, 0.993 (unitless)

Acknowledgments

= enter acknowledgments here =

References

Allen, C. D., A. K. Macalady, H. Chenchouni, D. Bachelet, N. McDowell, M. Vennetier, T. Kitzberger, A. Rigling, D. D. Breshears, E. T. Hogg, P. Gonzalez, R. Fensham, Z. Zhang, J. Castro, N. Demidova, J.-H. Lim, G. Allard, S. W. Running, A. Semerci, and N. Cobb (2010), A global overview of drought and heat-induced tree mortality reveals emerging climate change risks for forests, *Forest Ecology and Management*, 259(4), 660 – 684, doi:https://doi.org/10.1016/j.foreco.2009.09.001.

Anderegg, W. R. L. (2015a), Spatial and temporal variation in plant hydraulic traits and their relevance for climate change impacts on vegetation, *New Phytologist*, 205(3), 1008–1014, doi:10.1111/nph.12907.

Anderegg, W. R. L., J. M. Kane, and L. D. L. Anderegg (2013a), Consequences of widespread tree mortality triggered by drought and temperature stress, *Nature Climate Change*, 3(1), 30–36.

Anderegg, W. R. L., L. Plavcová, L. D. L. Anderegg, U. G. Hacke, J. A. Berry, and C. B. Field (2013b), Drought's legacy: multiyear hydraulic deterioration underlies widespread

aspen forest die-off and portends increased future risk, *Global Change Biology*, *19*(4), 1188–1196, doi:10.1111/gcb.12100.

Anderegg, W. R. L., C. Schwalm, F. Biondi, J. J. Camarero, G. Koch, M. Litvak, K. Ogle, J. D. Shaw, E. Shevliakova, A. P. Williams, A. Wolf, E. Ziaco, and S. Pacala (2015b), Pervasive drought legacies in forest ecosystems and their implications for carbon cycle models, *Science*, *349*(6247), 528–532, doi:10.1126/science.aab1833.

Anderegg, W. R. L., A. Wolf, A. Arango-Velez, B. Choat, D. J. Chmura, S. Jansen, T. Kolb, S. Li, F. Meinzer, P. Pita, V. Resco de Dios, J. S. Sperry, B. T. Wolfe, and S. Pacala (2017), Plant water potential improves prediction of empirical stomatal models, *PLOS ONE*, *12*(10), 1–17, doi:10.1371/journal.pone.0185481.

Avissar, R., P. L. Silva Dias, M. A. F. Silva Dias, and C. Nobre (2002), The large-scale biosphere-atmosphere experiment in Amazonia (LBA): Insights and future research needs, *Journal of Geophysical Research: Atmospheres*, *107*(D20), LBA 54–1–LBA 54–6, doi: 10.1029/2002JD002704.

Bartlett, M. K., T. Klein, S. Jansen, B. Choat, and L. Sack (2016), The correlations and sequence of plant stomatal, hydraulic, and wilting responses to drought, *Proceedings of the National Academy of Sciences*, *113*(46), 13,098–13,103, doi:10.1073/pnas.1604088113.

Bohrer, G., H. Mourad, T. A. Laursen, D. Drewry, R. Avissar, D. Poggi, R. Oren, and G. G. Katul (2005), Finite element tree crown hydrodynamics model (FETCH) using porous media flow within branching elements: A new representation of tree hydrodynamics, *Water Resources Research*, *41*(11), doi:10.1029/2005WR004181.

Bonan, G. B. (2008), Forests and climate change: Forcings, feedbacks, and the climate benefits of forests, *Science*, *320*(5882), 1444–1449, doi:10.1126/science.1155121.

Bonan, G. B., P. J. Lawrence, K. W. Oleson, S. Levis, M. Jung, M. Reichstein, D. M. Lawrence, and S. C. Swenson (2011), Improving canopy processes in the Community Land Model version 4 (CLM4) using global flux fields empirically inferred from FLUXNET data, *Journal of Geophysical Research*, *116*, doi:10.1029/2010JG001593.

Bonan, G. B., M. Williams, R. A. Fisher, and K. W. Oleson (2014), Modeling stomatal conductance in the earth system: linking leaf water-use efficiency and water transport along the soil-plant-atmosphere continuum, *Geoscientific Model Development*, *7*(5), 2193–2222, doi:10.5194/gmd-7-2193-2014.

Bouda, M., and J. E. Saiers (2017), Dynamic effects of root system architecture improve root water uptake in 1-d process-based soil-root hydrodynamics, *Advances in Water Resources*, *110*, 319 – 334, doi:https://doi.org/10.1016/j.advwatres.2017.10.018.

Boyer, J. S. (1967), Leaf water potentials measured with a pressure chamber, *Plant Physiology*, *42*(1), 133–137, doi:10.1104/pp.42.1.133.

Brooks, J. R., F. C. Meinzer, J. M. Warren, J.-C. Domec, and R. Coulombe (2006), Hydraulic redistribution in a Douglas-fir forest: lessons from system manipulations, *Plant, Cell & Environment*, *29*(1), 138–150, doi:10.1111/j.1365-3040.2005.01409.x.

Brooks, R., and A. Corey (1964), *Hydraulic Properties of Porous Media*, Colorado State University Hydrology Papers, Colorado State University.

Burgess, S. S. O., M. A. Adams, N. C. Turner, and C. K. Ong (1998), The redistribution of soil water by tree root systems, *Oecologia*, *115*(3), 306–311, doi:10.1007/s004420050521.

Cai, G., J. Vanderborght, M. Langensiepen, A. Schnepf, H. Hüging, and H. Vereecken (2018), Root growth, water uptake, and sap flow of winter wheat in response to different soil water conditions, *Hydrology and Earth System Sciences*, *22*(4), 2449–2470, doi: 10.5194/hess-22-2449-2018.

Cai, W., S. Borlace, M. Lengaigne, P. Van Rensch, M. Collins, G. Vecchi, A. Timmermann, A. Santoso, M. J. Mcphaden, L. Wu, M. H. England, G. Wang, E. Guilyardi, and F.-f. Jin (2014), Increasing frequency of extreme El Niño events due to greenhouse warming, *Nature Climate Change*, *4*(2), 111–116.

Celia, M. A., E. T. Bouloutas, and R. L. Zarba (1990), A general mass-conservative numerical solution for the unsaturated flow equation, *Water Resources Research*, *26*(7), 1483–1496, doi:10.1029/WR026i007p01483.

Choat, B., S. Jansen, T. J. Brodribb, H. Cochard, S. Delzon, R. Bhaskar, S. J. Bucci, T. S. Feild, S. M. Gleason, U. G. Hacke, A. L. Jacobsen, F. Lens, H. Maherali, J. Martínez-Vilalta, S. Mayr, M. Mencuccini, P. J. Mitchell, A. Nardini, J. Pittermann, R. B. Pratt, J. S. Sperry, M. Westoby, I. J. Wright, and A. E. Zanne (2012), Global convergence in the vulnerability of forests to drought, *Nature*, *491*(7426), 752–5.

Christoffersen, B. O., M. Gloor, S. Fauset, N. M. Fyllas, D. R. Galbraith, T. R. Baker, B. Kruijt, L. Rowland, R. A. Fisher, O. J. Binks, S. Sevanto, C. Xu, S. Jansen, B. Choat, M. Mencuccini, N. G. McDowell, and P. Meir (2016), Linking hydraulic traits to tropical forest function in a size-structured and trait-driven model (TFS v.1-Hydro), *Geoscientific Model Development*, *9*(11), 4227–4255, doi:10.5194/gmd-9-4227-2016.

Clapp, R. B., and G. M. Hornberger (1978), Empirical equations for some soil hydraulic properties, *Water Resources Research*, *14*(4), 601–604, doi:10.1029/WR014i004p00601.

Collatz, G., J. Ball, C. Grivet, and J. A. Berry (1991), Physiological and environmental regulation of stomatal conductance, photosynthesis and transpiration: a model that includes a laminar boundary layer, *Agricultural and Forest Meteorology*, *54*(2), 107 – 136, doi: http://dx.doi.org/10.1016/0168-1923(91)90002-8.

da Costa, A. C., D. B. Metcalfe, C. E. Doughty, A. A. de Oliveira, G. F. Neto, M. C. da Costa, J. de Athaydes Silva Junior, L. E. Aragão, S. Almeida, D. R. Galbraith, L. M. Rowland, P. Meir, and Y. Malhi (2014), Ecosystem respiration and net primary productivity after 8-10 years of experimental through-fall reduction in an eastern Amazon forest, *Plant Ecology & Diversity*, *7*(1-2), 7–24, doi:10.1080/17550874.2013.798366.

da Costa, A. C. L., D. Galbraith, S. Almeida, B. Takeshi, T. Portela, M. da Costa, J. ao de Athaydes Silva Junior, A. P. Braga, P. H. L. de Gonçalves, A. A. de Oliveira, R. Fisher, O. L. Phillips, D. B. Metcalfe, P. Levy, and P. Meir (2010), Effect of 7 yr of experimental drought on vegetation dynamics and biomass storage of an eastern Amazonian rainforest, *The New Phytologist*, *187*(3), 579–591.

Dai, Y., R. E. Dickinson, and Y.-P. Wang (2004), A two-big-leaf model for canopy temperature, photosynthesis, and stomatal conductance, *Journal of Climate*, *17*(12), 2281–2299, doi:10.1175/1520-0442(2004)017<2281:ATMFCT>2.0.CO;2.

De Kauwe, M. G., J. Kala, Y.-S. Lin, A. J. Pitman, B. E. Medlyn, R. A. Duursma, G. Abramowitz, Y.-P. Wang, and D. G. Miralles (2015), A test of an optimal stomatal conductance scheme within the CABLE land surface model, *Geoscientific Model Development*, *8*(2), 431–452, doi:10.5194/gmd-8-431-2015.

De Kauwe, M. G., B. E. Medlyn, J. Knauer, and C. A. Williams (2017), Ideas and perspectives: how coupled is the vegetation to the boundary layer?, *Biogeosciences*, *14*(19), 4435–4453, doi:10.5194/bg-14-4435-2017.

Domec, J.-C., J. S. King, A. Noormets, E. Treasure, M. J. Gavazzi, G. Sun, and S. G. Mc-Nulty (2010), Hydraulic redistribution of soil water by roots affects whole-stand evapotranspiration and net ecosystem carbon exchange, *The New Phytologist*, *187*(1), 171–183, doi:10.1111/j.1469-8137.2010.03245.x.

Drake, J., S. Power, R. Duursma, B. Medlyn, M. Aspinwall, B. Choat, D. Creek, D. Eamus, C. Maier, S. Pfautsch, R. Smith, M. Tjoelker, and D. Tissue (2017), Stomatal and non-stomatal limitations of photosynthesis for four tree species under drought: A comparison of model formulations, *Agricultural and Forest Meteorology*, *247*, 454 – 466, doi: https://doi.org/10.1016/j.agrformet.2017.08.026.

Egea, G., A. Verhoef, and P. L. Vidale (2011), Towards an improved and more flexible representation of water stress in coupled photosynthesis-stomatal conductance models, *Agricultural and Forest Meteorology*, *151*(10), 1370 – 1384, doi: https://doi.org/10.1016/j.agrformet.2011.05.019.

Entekhabi, D., E. G. Njoku, P. E. O'Neill, K. H. Kellogg, W. T. Crow, W. N. Edelstein, J. K. Entin, S. D. Goodman, T. J. Jackson, J. Johnson, J. Kimball, J. R. Piepmeier, R. D. Koster, N. Martin, K. C. McDonald, M. Moghaddam, S. Moran, R. Reichle, J. C. Shi, M. W. Spencer, S. W. Thurman, L. Tsang, and J. V. Zyl (2010), The soil moisture active passive (SMAP) mission, *Proceedings of the IEEE*, *98*(5), 704–716, doi:

10.1109/JPROC.2010.2043918.

Epila, J., N. J. De Baerdemaeker, L. L. Vergeynst, W. H. Maes, H. Beeckman, and K. Steppe (2017), Capacitive water release and internal leaf water relocation delay drought-induced cavitation in African Maesopsis eminii, *Tree Physiology*, *37*(4), 481–490, doi: 10.1093/treephys/tpw128.

Farquhar, G. D., S. von Caemmerer, and J. A. Berry (1980), A biochemical model of photosynthetic CO_2 assimilation in leaves of C_3 species, *Planta*, *149*(1), 78–90, doi: 10.1007/BF00386231.

Ficklin, D. L., and K. A. Novick (2017), Historic and projected changes in vapor pressure deficit suggest a continental-scale drying of the United States atmosphere, *Journal of Geophysical Research: Atmospheres*, *122*(4), 2061–2079, doi:10.1002/2016JD025855.

Fisher, R. A., M. Williams, R. L. Do Vale, A. L. Da Costa, and P. Meir (2006), Evidence from Amazonian forests is consistent with isohydric control of leaf water potential, *Plant, Cell & Environment*, *29*(2), 151–165, doi:10.1111/j.1365-3040.2005.01407.x.

Fisher, R. A., M. Williams, A. L. D. Costa, Y. Malhi, R. F. D. Costa, S. Almeida, and P. Meir (2007), The response of an Eastern Amazonian rain forest to drought stress: results and modelling analyses from a throughfall exclusion experiment, *Global Change Biology*, *13*(11), 2361–2378, doi:10.1111/j.1365-2486.2007.01417.x.

Fisher, R. A., M. Williams, M. de Lourdes Ruivo, A. L. de Costa, and P. Meir (2008), Evaluating climatic and soil water controls on evapotranspiration at two Amazonian rainforest sites, *Agricultural and Forest Meteorology*, *148*(6), 850 – 861, doi: https://doi.org/10.1016/j.agrformet.2007.12.001.

Flexas, J., J. Bota, F. Loreto, G. Cornic, and T. D. Sharkey (2004), Diffusive and metabolic limitations to photosynthesis under drought and salinity in C3 plants, *Plant Biology*, *6*(3), 269–279, doi:10.1055/s-2004-820867.

Flexas, J., M. Ribas-Carbó, J. Bota, J. Galmés, M. Henkle, S. Martínez-Cañellas, and H. Medrano (2006), Decreased rubisco activity during water stress is not induced by decreased relative water content but related to conditions of low stomatal conductance and chloroplast CO2 concentration, *New Phytologist*, *172*(1), 73–82, doi:10.1111/j.1469-8137.2006.01794.x.

Flexas, J., M. M. Barbour, O. Brendel, H. M. Cabrera, M. Carriquí, A. Díaz-Espejo, C. Douthe, E. Dreyer, J. P. Ferrio, J. Gago, A. Gallé, J. Galmés, N. Kodama, H. Medrano, Ü. Niinemets, J. J. Peguero-Pina, A. Pou, M. Ribas-Carbó, M. Tomás, T. Tosens, and C. R. Warren (2012), Mesophyll diffusion conductance to CO2: An unappreciated central player in photosynthesis, *Plant Science*, *193-194*, 70 – 84, doi: https://doi.org/10.1016/j.plantsci.2012.05.009.

Franks, P. J., P. L. Drake, and R. H. Froend (2007), Anisohydric but isohydrodynamic: seasonally constant plant water potential gradient explained by a stomatal control mechanism incorporating variable plant hydraulic conductance, *Plant, Cell & Environment*, *30*(1), 19–30, doi:10.1111/j.1365-3040.2006.01600.x.

Friedlingstein, P., M. Meinshausen, V. K. Arora, C. D. Jones, A. Anav, S. K. Liddicoat, and R. Knutti (2014), Uncertainties in CMIP5 climate projections due to carbon cycle feedbacks, *Journal of Climate*, *27*(2), 511–526.

Fu, R., L. Yin, W. Li, P. A. Arias, R. E. Dickinson, L. Huang, S. Chakraborty, K. Fernandes, B. Liebmann, R. Fisher, and R. B. Myneni (2013), Increased dry-season length over southern Amazonia in recent decades and its implication for future climate projection, *Proceedings of the National Academy of Sciences of the United States of America*, *110*(45), 18,110–18,115.

Gentine, P., D. Entekhabi, A. Chehbouni, G. Boulet, and B. Duchemin (2007), Analysis of evaporative fraction diurnal behaviour, *Agricultural and Forest Meteorology*, *143*(1), 13 – 29, doi:https://doi.org/10.1016/j.agrformet.2006.11.002.

Gentine, P., D. Entekhabi, and J. Polcher (2011), The diurnal behavior of evaporative fraction in the soil-vegetation-atmospheric boundary layer continuum, *Journal of Hydrometeorology*, *12*(6), 1530–1546, doi:10.1175/2011JHM1261.1.

Gentine, P., M. Guérin, M. Uriarte, N. G. McDowell, and W. T. Pockman (2016), An allometry-based model of the survival strategies of hydraulic failure and carbon starvation, *Ecohydrology*, *9*(3), 529–546, doi:10.1002/eco.1654.

Giardina, F., A. G. Konings, D. Kennedy, S. H. Alemohammad, R. S. Oliveira, M. Uriarte, and P. Gentine (2018), Tall Amazonian forests are less sensitive to precipitation variability, *Nature Geoscience*, *11*(6), 405–409, doi:10.1038/s41561-018-0133-5.

Grant, J., J.-P. Wigneron, R. D. Jeu, H. Lawrence, A. Mialon, P. Richaume, A. A. Bitar, M. Drusch, M. van Marle, and Y. Kerr (2016), Comparison of SMOS and AMSR-E vegetation optical depth to four MODIS-based vegetation indices, *Remote Sensing of Environment*, *172*, 87 – 100, doi:https://doi.org/10.1016/j.rse.2015.10.021.

Green, J. K., A. G. Konings, S. H. Alemohammad, J. Berry, D. Entekhabi, J. Kolassa, J.-E. Lee, and P. Gentine (2017), Regionally strong feedbacks between the atmosphere and terrestrial biosphere, *Nature Geoscience*, *10*(6), 410–414, doi:10.1038/ngeo2957.

Harley, P. C., R. B. Thomas, J. F. Reynolds, and B. R. Strain (1992), Modelling photosynthesis of cotton grown in elevated CO2, *Plant Cell Environment*, *15*(3), 271–282, doi:10.1111/j.1365-3040.1992.tb00974.x.

Holbrook, N. M., E. T. Ahrens, M. J. Burns, and M. A. Zwieniecki (2001), In vivo observation of cavitation and embolism repair using magnetic resonance imaging, *Plant Physiology*, *126*(1), 27–31, doi:10.1104/pp.126.1.27.

Huntingford, C., P. Zelazowski, D. Galbraith, L. M. Mercado, S. Sitch, R. Fisher, M. Lomas, A. P. Walker, C. D. Jones, B. B. B. Booth, Y. Malhi, D. Hemming, G. Kay, P. Good, S. L. Lewis, O. L. Phillips, O. K. Atkin, J. Lloyd, E. Gloor, J. Zaragoza-castells, P. Meir, R. Betts, P. P. Harris, C. Nobre, J. Marengo, and P. M. Cox (2013), Simulated resilience of tropical rainforests to CO2-induced climate change, *Nature Geoscience*, *6*(4), 268–273.

Jackson, R. B., J. Canadell, J. R. Ehleringer, H. A. Mooney, O. E. Sala, and E. D. Schulze (1996), A global analysis of root distributions for terrestrial biomes, *Oecologia*, *108*(3), 389–411, doi:10.1007/BF00333714.

Jackson, R. B., J. S. Sperry, and T. E. Dawson (2000), Root water uptake and transport: using physiological processes in global predictions, *Trends in Plant Science*, *5*(11), 482 – 488, doi:https://doi.org/10.1016/S1360-1385(00)01766-0.

Jarvis, N. J. (2011), Simple physics-based models of compensatory plant water uptake: concepts and eco-hydrological consequences, *Hydrology and Earth System Sciences*, *15*(11), 3431–3446, doi:10.5194/hess-15-3431-2011.

Joetzjer, E., C. Delire, H. Douville, P. Ciais, B. Decharme, R. Fisher, B. Christoffersen, J. C. Calvet, A. C. L. da Costa, L. V. Ferreira, and P. Meir (2014), Predicting the response of the Amazon rainforest to persistent drought conditions under current and future climates: a major challenge for global land surface models, *Geoscientific Model Development*, *7*(6), 2933–2950, doi:10.5194/gmd-7-2933-2014.

Kattge, J., S. Díaz, S. Lavorel, I. C. Prentice, and et al. (2011), TRY - a global database of plant traits, *Global Change Biology*, *17*(9), 2905–2935, doi:10.1111/j.1365-2486.2011.02451.x.

Keenan, T., R. García, A. D. Friend, S. Zaehle, C. Gracia, and S. Sabate (2009), Improved understanding of drought controls on seasonal variation in Mediterranean forest canopy CO_2 and water fluxes through combined in situ measurements and ecosystem modelling, *Biogeosciences*, *6*(8), 1423–1444, doi:10.5194/bg-6-1423-2009.

Keenan, T., I. Baker, A. Barr, P. Ciais, K. Davis, M. Dietze, D. Dragoni, C. M. Gough, R. Grant, D. Hollinger, K. Hufkens, B. Poulter, H. McCaughey, B. Raczka, Y. Ryu, K. Schaefer, H. Tian, H. Verbeeck, M. Zhao, and A. D. Richardson (2012), Terrestrial biosphere model performance for inter-annual variability of land-atmosphere CO2 exchange, *Global Change Biology*, *18*(6), 1971–1987, doi:10.1111/j.1365-2486.2012.02678.x.

Klein, T., and S. Niu (2014), The variability of stomatal sensitivity to leaf water potential across tree species indicates a continuum between isohydric and anisohydric behaviours, *Functional Ecology*, *28*(6), 1313–1320, doi:10.1111/1365-2435.12289.

Konings, A. G., and P. Gentine (2017a), Global variations in ecosystem-scale isohydricity, *Global Change Biology*, *23*(2), 891–905, doi:10.1111/gcb.13389.

Konings, A. G., M. Piles, K. Rötzer, K. A. McColl, S. K. Chan, and D. Entekhabi (2016), Vegetation optical depth and scattering albedo retrieval using time series of dual-polarized l-band radiometer observations, *Remote Sensing of Environment*, *172*, 178 – 189, doi: https://doi.org/10.1016/j.rse.2015.11.009.

Konings, A. G., A. P. Williams, and P. Gentine (2017b), Sensitivity of grassland productivity to aridity controlled by stomatal and xylem regulation, *Nature Geoscience*, *10*(4), 284–288, doi:10.1038/ngeo2903.

Kotowska, M. M., D. Hertel, Y. A. Rajab, H. Barus, and B. Schuldt (2015), Patterns in hydraulic architecture from roots to branches in six tropical tree species from cacao agroforestry and their relation to wood density and stem growth, *Frontiers in Plant Science*, *6*, 191, doi:10.3389/fpls.2015.00191.

Lee, J.-E., R. S. Oliveira, T. E. Dawson, and I. Fung (2005), Root functioning modifies seasonal climate, *Proceedings of the National Academy of Sciences of the United States of America*, *102*(49), 17,576–17,581, doi:10.1073/pnas.0508785102.

Lemordant, L., P. Gentine, A. S. Swann, B. I. Cook, and J. Scheff (2018), Critical impact of vegetation physiology on the continental hydrologic cycle in response to increasing CO2, *Proceedings of the National Academy of Sciences*, doi:10.1073/pnas.1720712115.

Lin, C., P. Gentine, Y. Huang, K. Guan, H. Kimm, and S. Zhou (2018), Diel ecosystem conductance response to vapor pressure deficit is suboptimal and independent of soil moisture, *Agricultural and Forest Meteorology*, *250-251*, 24 – 34, doi: https://doi.org/10.1016/j.agrformet.2017.12.078.

Mackay, D. S., D. E. Roberts, B. E. Ewers, J. S. Sperry, N. G. McDowell, and W. T. Pockman (2015), Interdependence of chronic hydraulic dysfunction and canopy processes can improve integrated models of tree response to drought, *Water Resources Research*, *51*(8), 6156–6176, doi:10.1002/2015WR017244.

Manzoni, S., G. Vico, G. Katul, P. A. Fay, W. Polley, S. Palmroth, and A. Porporato (2011), Optimizing stomatal conductance for maximum carbon gain under water stress: a meta-analysis across plant functional types and climates, *Functional Ecology*, *25*(3), 456–467, doi:10.1111/j.1365-2435.2010.01822.x.

Manzoni, S., G. Vico, G. Katul, S. Palmroth, R. B. Jackson, and A. Porporato (2013a), Hydraulic limits on maximum plant transpiration and the emergence of the safety-efficiency trade-off, *New Phytologist*, *198*(1), 169–178, doi:10.1111/nph.12126.

Manzoni, S., G. Vico, S. Palmroth, A. Porporato, and G. Katul (2013b), Optimization of stomatal conductance for maximum carbon gain under dynamic soil moisture, *Advances in Water Resources*, *62*, 90 – 105, doi:https://doi.org/10.1016/j.advwatres.2013.09.020.

McDowell, N., C. D. Allen, K. Anderson-Teixeira, P. Brando, R. Brienen, J. Chambers, B. Christoffersen, S. Davies, C. Doughty, A. Duque, F. Espirito-Santo, R. Fisher, C. G. Fontes, D. Galbraith, D. Goodsman, C. Grossiord, H. Hartmann, J. Holm, D. J. Johnson, A. R. Kassim, M. Keller, C. Koven, L. Kueppers, T. Kumagai, Y. Malhi, S. M. McMahon, M. Mencuccini, P. Meir, P. Moorcroft, M.-L. H. C., O. L. Phillips, T. Powell, C. A. Sierra, J. Sperry, J. Warren, C. Xu, and X. Xu (2018), Drivers and mechanisms of tree mortality in moist tropical forests, *New Phytologist*, *219*(3), 851–869, doi:10.1111/nph.15027.

McDowell, N. G., and C. D. Allen (2015), Darcy's law predicts widespread forest mortality under climate warming, *Nature Climate Change*, *5*(7), 669–672.

McDowell, N. G., R. A. Fisher, C. Xu, J. C. Domec, T. Hölttä, D. S. Mackay, J. S. Sperry, A. Boutz, L. Dickman, N. Gehres, J. M. Limousin, A. Macalady, J. Martínez-Vilalta, M. Mencuccini, J. A. Plaut, J. Ogée, R. E. Pangle, D. P. Rasse, M. G. Ryan, S. Sevanto, R. H. Waring, A. P. Williams, E. A. Yepez, and W. T. Pockman (2013), Evaluating theories of drought-induced vegetation mortality using a multimodel-experiment framework, *New Phytologist*, *200*(2), 304–321, doi:10.1111/nph.12465.

McDowell, N. G., A. P. Williams, C. Xu, W. T. Pockman, L. T. Dickman, S. Sevanto, R. Pangle, J. Limousin, J. Plaut, D. S. Mackay, J. Ogee, J. C. Domec, C. D. Allen, R. A. Fisher,

X. Jiang, J. D. Muss, D. D. Breshears, S. A. Rauscher, and C. Koven (2016), Multi-scale predictions of massive conifer mortality due to chronic temperature rise, *Nature Climate Change*, 6, 295–300, doi:10.1038/nclimate2873.

Medlyn, B. E., R. A. Duursma, D. Eamus, D. S. Ellsworth, I. C. Prentice, C. V. M. Barton, K. Y. Crous, P. De Angelis, M. Freeman, and L. Wingate (2011), Reconciling the optimal and empirical approaches to modelling stomatal conductance, *Global Change Biology*, 17(6), 2134–2144, doi:10.1111/j.1365-2486.2010.02375.x.

Meinzer, F. C., S. A. James, and G. Goldstein (2004), Dynamics of transpiration, sap flow and use of stored water in tropical forest canopy trees, *Tree Physiology*, 24(8), 901–909, doi:10.1093/treephys/24.8.901.

Meinzer, F. C., D. M. Johnson, B. Lachenbruch, K. A. McCulloh, and D. R. Woodruff (2009), Xylem hydraulic safety margins in woody plants: coordination of stomatal control of xylem tension with hydraulic capacitance, *Functional Ecology*, 23(5), 922–930, doi:10.1111/j.1365-2435.2009.01577.x.

Momen, M., J. D. Wood, K. A. Novick, R. Pangle, W. T. Pockman, N. G. McDowell, and A. G. Konings (2017), Interacting effects of leaf water potential and biomass on vegetation optical depth, *Journal of Geophysical Research: Biogeosciences*, 122(11), 3031–3046, doi:10.1002/2017JG004145.

Nepstad, D. C., R. de Carvalho, Claudio, E. A. Davidson, P. H. Jipp, P. A. Lefebvre, G. H. Negreiros, E. D. da Silva, T. A. Stone, S. E. Trumbore, and S. Vieira (1994), The role of deep roots in the hydrological and carbon cycles of Amazonian forests and pastures, *Nature*, 372(6507), 666.

Novick, K. A., D. L. Ficklin, P. C. Stoy, C. A. Williams, G. Bohrer, A. Oishi, S. A. Papuga, P. D. Blanken, A. Noormets, B. N. Sulman, R. L. Scott, L. Wang, and R. P. Phillips (2016a), The increasing importance of atmospheric demand for ecosystem water and carbon fluxes, *Nature Climate Change*, 6(11), 1023–1027.

Novick, K. A., C. F. Miniat, and J. M. Vose (2016b), Drought limitations to leaf-level gas exchange: results from a model linking stomatal optimization and cohesion-tension theory, *Plant, Cell & Environment*, 39(3), 583–596, doi:10.1111/pce.12657.

Oleson, K. W., D. M. Lawrence, G. B. Bonan, B. Drewniak, M. Huang, C. D. Koven, S. Levis, F. Li, W. J. Riley, Z. M. Subin, S. C. Swenson, P. E. Thornton, A. Bozbiyik, R. Fisher, C. L. Heald, E. Kluzek, J.-F. Lamarque, P. J. Lawrence, L. R. Leung, W. Lipscomb, S. Muszala, D. M. Ricciuto, W. Sacks, Y. Sun, J. Tang, and Z.-L. Yang (2013), Technical description of version 4.5 of the Community Land Model (CLM), NCAR Tech. Note NCAR/TN-503+STR, *National Center for Atmospheric Research, Boulder, Colorado, 420 pp.*, doi:10.5065/D6RR1W7M.

Oliveira, R. S., T. E. Dawson, S. S. O. Burgess, and D. C. Nepstad (2005), Hydraulic redistribution in three amazonian trees, *Oecologia*, 145(3), 354–363, doi:10.1007/s00442-005-0108-2.

Powell, T. L., D. R. Galbraith, B. O. Christoffersen, A. Harper, H. M. A. Imbuzeiro, L. Rowland, S. Almeida, P. M. Brando, A. C. L. da Costa, M. H. Costa, N. M. Levine, Y. Malhi, S. R. Saleska, E. Sotta, M. Williams, P. Meir, and P. R. Moorcroft (2013), Confronting model predictions of carbon fluxes with measurements of amazon forests subjected to experimental drought, *New Phytologist*, 200(2), 350–365, doi:10.1111/nph.12390.

Powell, T. L., W. J. K., O. A. A. R., C. A. C. Lola, S. S. R., M. Patrick, and M. P. R. (2018), Differences in xylem and leaf hydraulic traits explain differences in drought tolerance among mature amazon rainforest trees, *Global Change Biology*, 23(10), 4280–4293, doi: 10.1111/gcb.13731.

Restaino, C. M., D. L. Peterson, and J. Littell (2016), Increased water deficit decreases Douglas fir growth throughout western US forests, *Proceedings of the National Academy of Sciences*, 113(34), 9557–9562, doi:10.1073/pnas.1602384113.

Restrepo-Coupe, N., N. M. Levine, B. O. Christoffersen, L. P. Albert, J. Wu, M. H. Costa, D. Galbraith, H. Imbuzeiro, G. Martins, A. C. da Araujo, Y. S. Malhi, X. Zeng, P. Moorcroft, and S. R. Saleska (2017), Do dynamic global vegetation models capture the season-

ality of carbon fluxes in the amazon basin? A data-model intercomparison, *Global Change Biology*, *23*(1), 191–208, doi:10.1111/gcb.13442.

Rogers, A., B. E. Medlyn, J. S. Dukes, G. Bonan, S. Caemmerer, M. C. Dietze, J. Kattge, A. D. B. Leakey, L. M. Mercado, Ü. Niinemets, I. C. Prentice, S. P. Serbin, S. Sitch, D. A. Way, and S. Zaehle (2017), A roadmap for improving the representation of photosynthesis in Earth system models, *New Phytologist*, *213*(1), 22–42, doi:10.1111/nph.14283.

Rowland, L., A. da Costa, D. R. Galbraith, R. S. Oliveira, O. J. Binks, A. A. R. Oliveira, A. M. Pullen, C. E. Doughty, D. B. Metcalfe, S. S. Vasconcelos, L. V. Ferreira, Y. Malhi, J. Grace, M. Mencuccini, and P. Meir (2015), Death from drought in tropical forests is triggered by hydraulics not carbon starvation, *Nature*, *528*(7580), 119–122I.

Sack, L., P. J. Melcher, M. A. Zwieniecki, and N. M. Holbrook (2002), The hydraulic conductance of the angiosperm leaf lamina: a comparison of three measurement methods, *Journal of Experimental Botany*, *53*(378), 2177–2184.

Scholz, F. G., N. G. Phillips, S. J. Bucci, F. C. Meinzer, and G. Goldstein (2011), Hydraulic capacitance: Biophysics and functional significance of internal water sources, in Meinzer, F.C., Lachenbruch, B., Dawson, T. E. (eds) *Size- and Age-Related Changes in Tree Structure and Function*, pp. 341–361, Springer, Dordrecht.

Seager, R., A. Hooks, A. P. Williams, B. Cook, J. Nakamura, and N. Henderson (2015), Climatology, variability, and trends in the U.S. vapor pressure deficit, an important fire-related meteorological quantity, *Journal of Applied Meteorology and Climatology*, *54*(6), 1121–1141, doi:10.1175/JAMC-D-14-0321.1.

Sellers, P. J., D. A. Randall, G. J. Collatz, J. A. Berry, C. B. Field, D. A. Dazlich, C. Zhang, G. D. Collelo, and L. Bounoua (1996a), a revised land surface parameterization (SiB2) for atmospheric GCMs. part I: Model formulation, *Journal of Climate*, *9*(4), 676–705, doi:10.1175/1520-0442(1996)009<0676:ARLSPF>2.0.CO;2.

Sellers, P. J., C. J. Tucker, G. J. Collatz, S. O. Los, C. O. Justice, D. A. Dazlich, and D. A. Randall (1996b), A revised land surface parameterization (SiB2) for atmospheric GCMs. part II: The generation of global fields of terrestrial biophysical parameters from satellite data, *Journal of Climate*, *9*(4), 706–737, doi:10.1175/1520-0442(1996)009<0706:ARLSPF>2.0.CO;2.

Seneviratne, S. I., D. Lüthi, M. Litschi, and C. Schär (2006), Land-atmosphere coupling and climate change in Europe, *Nature*, *443*(7108), 205–9.

Simonin, K. A., E. Burns, B. Choat, M. M. Barbour, T. E. Dawson, and P. J. Franks (2015), Increasing leaf hydraulic conductance with transpiration rate minimizes the water potential drawdown from stem to leaf, *Journal of Experimental Botany*, *66*(5), 1303–1315, doi:10.1093/jxb/eru481.

Siqueira, M., G. Katul, and A. Porporato (2008), Onset of water stress, hysteresis in plant conductance, and hydraulic lift: Scaling soil water dynamics from millimeters to meters, *Water Resources Research*, *44*(1), W01,432, doi:10.1029/2007WR006094.

Sperry, J. S., and D. M. Love (2015), What plant hydraulics can tell us about responses to climate-change droughts, *New Phytologist*, *207*(1), 14–27, doi:10.1111/nph.13354.

Sperry, J. S., F. R. Adler, G. S. Campbell, and J. P. Comstock (1998), Limitation of plant water use by rhizosphere and xylem conductance: results from a model, *Plant Cell Environment*, *21*(4), 347–359, doi:10.1046/j.1365-3040.1998.00287.x.

Sperry, J. S., U. G. Hacke, R. Oren, and J. P. Comstock (2002), Water deficits and hydraulic limits to leaf water supply, *Plant, Cell & Environment*, *25*(2), 251–263, doi:10.1046/j.0016-8025.2001.00799.x.

Sperry, J. S., M. D. Venturas, W. R. L. Anderegg, M. Mencuccini, D. S. Mackay, Y. Wang, and D. M. Love (2017), Predicting stomatal responses to the environment from the optimization of photosynthetic gain and hydraulic cost, *Plant, Cell & Environment*, *40*(6), 816–830, doi:10.1111/pce.12852, pCE-16-0541.R1.

Tang, J., W. J. Riley, and J. Niu (2015), Incorporating root hydraulic redistribution in CLM4.5: Effects on predicted site and global evapotranspiration, soil moisture, and water storage, *Journal of Advances in Modeling Earth Systems*, *7*(4), 1828–1848, doi:

10.1002/2015MS000484.

Tardieu, F., and T. Simonneau (1998), Variability among species of stomatal control under fluctuating soil water status and evaporative demand: modelling isohydric and anisohydric behaviours, *Journal of Experimental Botany*, *49*, 419–432.

Thornton, P. E., and N. E. Zimmermann (2007), An improved canopy integration scheme for a land surface model with prognostic canopy structure, *Journal of Climate*, *20*(15), 3902–3923, doi:10.1175/JCLI4222.1.

Trugman, A. T., D. Medvigy, J. S. Mankin, and W. R. L. Anderegg (2018), Soil moisture stress as a major driver of carbon cycle uncertainty, *Geophysical Research Letters*, *45*, doi:10.1029/2018GL078131.

Tyree, M. T., and J. S. Sperry (1988), Do woody plants operate near the point of catastrophic xylem dysfunction caused by dynamic water stress?: Answers from a model, *Plant Physiology*, *88*(3), 574–580.

Tyree, M. T., and J. S. Sperry (1989), Vulnerability of xylem to cavitation and embolism, *Annual Review of Plant Physiology and Plant Molecular Biology*, *40*(1), 19–36, doi:10.1146/annurev.pp.40.060189.000315.

Ukkola, A. M., M. G. D. Kauwe, A. J. Pitman, M. J. Best, G. Abramowitz, V. Haverd, M. Decker, and N. Haughton (2016), Land surface models systematically overestimate the intensity, duration and magnitude of seasonal-scale evaporative droughts, *Environmental Research Letters*, *11*(10), 104,012.

Verhoef, A., and G. Egea (2014), Modeling plant transpiration under limited soil water: Comparison of different plant and soil hydraulic parameterizations and preliminary implications for their use in land surface models, *Agricultural and Forest Meteorology*, *191*, 22–32, doi:https://doi.org/10.1016/j.agrformet.2014.02.009.

Warren, J. M., P. J. Hanson, C. M. Iversen, J. Kumar, A. P. Walker, and S. D. Wullschleger (2015), Root structural and functional dynamics in terrestrial biosphere models - evaluation and recommendations, *New Phytologist*, *205*(1), 59–78, doi:10.1111/nph.13034.

Williams, A. P., C. D. Allen, A. K. Macalady, D. Griffin, C. A. Woodhouse, D. M. Meko, T. W. Swetnam, S. A. Rauscher, R. Seager, H. Grissino-Mayer, J. S. Dean, E. R. Cook, C. Gangodagamage, M. Cai, and N. G. Mcdowell (2013), Temperature as a potent driver of regional forest drought stress and tree mortality, *Nature Climate Change*, *3*(3), 292–297.

Williams, M., E. B. Rastetter, D. N. Fernandes, M. L. Goulden, S. C. Wofsy, G. R. Shaver, J. M. Melillo, J. W. Munger, S.-M. Fan, and K. J. Nadelhoffer (1996), Modelling the soil-plant-atmosphere continuum in a Quercus-Acer stand at Harvard Forest: the regulation of stomatal conductance by light, nitrogen and soil/plant hydraulic properties, *Plant, Cell & Environment*, *19*(8), 911–927, doi:10.1111/j.1365-3040.1996.tb00456.x.

Williams, M., B. E. Law, P. M. Anthoni, and M. H. Unsworth (2001), Use of a simulation model and ecosystem flux data to examine carbon-water interactions in ponderosa pine., *Tree Physiology*, *21*(5), 287 – 298.

Xu, X., D. Medvigy, J. S. Powers, J. M. Becknell, and K. Guan (2016), Diversity in plant hydraulic traits explains seasonal and inter-annual variations of vegetation dynamics in seasonally dry tropical forests, *New Phytologist*, *212*(1), 80–95, doi:10.1111/nph.14009, 2015-20772.

Zhou, S., R. A. Duursma, B. E. Medlyn, J. W. Kelly, and I. C. Prentice (2013), How should we model plant responses to drought? An analysis of stomatal and non-stomatal responses to water stress, *Agricultural and Forest Meteorology*, *182-183*, 204 – 214, doi:https://doi.org/10.1016/j.agrformet.2013.05.009.

Zhou, S., B. Medlyn, S. Sabaté, D. Sperlich, I. C. Prentice, and D. Whitehead (2014), Short-term water stress impacts on stomatal, mesophyll and biochemical limitations to photosynthesis differ consistently among tree species from contrasting climates, *Tree Physiology*, *34*(10), 1035, doi:10.1093/treephys/tpu072.